Tunnelling and Underground Space Technology 92 (2019) 103061

Contents lists available at ScienceDirect

Tunnelling and Underground Space Technology

journal homepage: www.elsevier.com/locate/tust

Further development of the distinct lattice spring model for quasi-brittle crack propagation in concrete and its application in underground engineering

Qin Li, Gao-Feng Zhao, Jijian Lian*

State Key Laboratory of Hydraulic Engineering Simulation and Safety, School of Civil Engineering, Tianjin University, Tianjin, China

ARTICLE INFO

Keywords:
Distinct lattice spring model
Quasi-brittle crack propagation
Three-point bending test
Micromechanical constitutive model
Concrete lining

ABSTRACT

This paper further extends the ability of the distinct lattice spring model (DLSM) to predict quasi-brittle crack propagation in concrete. In contrast to brittle crack propagation, most experimental results confirm that the crack propagation in concrete is quasi-brittle. The DLSM was originally developed to study the brittle fracturing of rock. Whether and how it could be applied to quasi-brittle crack propagation has not been systematically studied. In this work, considering aspects of the geometric non-uniformity, material heterogeneity and micro-mechanical constitutive model, the ability of the DLSM to solve quasi-brittle crack propagation has been systematically investigated. The main contributions of this work are that it (1) confirmed the necessary for the DLSM to have a new micro-mechanical constitutive model to solve the quasi-brittle crack propagation problem; (2) established a new micro-mechanical constitutive model for quasi-brittle crack propagation; and (3) proposed a formula for the relationship between the micromechanical and macroscopic material parameters of the concrete. The new micromechanical constitutive model proposed in this paper has been systematically verified by three-point bending experimental results of various grades of concrete. Finally, the new constitutive model has been adopted to analyse the cracking of the concrete lining.

1. Introduction

Concrete is commonly used in underground engineering projects, and its cracking is closely related to the safety and durability of these projects. Strong external environmental changes, such as earthquakes and severe weather changes, may cause cracks in underground concrete structures, reducing its resistance and affecting its stability and safety (Mridha and Maity, 2014). Effectively estimating and predicting the crack initiation and propagation in concrete can better evaluate the stability and safety of underground engineering projects. Researchers have conducted numerous numerical and physical experiments on crack propagation in concrete (e.g., Huang, 2018; Zhu et al., 2002; Tang et al., 2015; Ooi et al., 2017). In contrast to traditional brittle crack propagation, both physical experiments and field observations have confirmed that crack propagation in concrete is highly nonlinear. For example, crack initiation and propagation in the concrete gravity dams demonstrate significant quasi-brittle properties, i.e. microcracking, inclusion toughening, surface roughness, and strain softening (Jenq and Shah, 1991, Omidi et al., 2013, Edalat-Behbahani et al., 2017, Wang et al., 2017a). This nonlinear cracking behaviour is called quasi-brittle crack propagation.

Numerical methods for quasi-brittle crack propagation in concrete can be divided into damage mechanics-based methods (Ghrib and Tinawi, 1995; Lee and Fenves, 1998; Calayir and Karaton, 2005; Omidi and Lotfi, 2013; Omidi et al., 2013) and fracture mechanics-based methods (Guanglun et al., 2000; Mirzabozorg and Ghaemian, 2005; Pan et al. 2011). Damage mechanics-based methods, such as the smear cracking method (Léger and Leclerc, 1996) and the plastic damage coupled model (Ghrib and Tinawi, 1995; Omidi et al., 2013), do not explicitly capture the crack surface but present the crack as the ultimate result of damage accumulation by using strain softening constitutive relations (Wang et al., 2017a). For example, in the smeared crack method (SCM) (de Borst, 2002), it is assumed that the length of the cracking process is related to the finite element size, the computational grid is set to remain constant, and the results are independent of the finite element mesh refinement. If the continuity of the displacement field does not reflect the discontinuous properties of the crack displacement, the SCM cannot predict the exact locations and propagation of the discrete cracks (Edalat-Behbahani et al., 2017). In addition, the SCM has the disadvantage of stress locking. To solve this problem, it is

* Corresponding author.
E-mail address: jjlian@tju.edu.cn (J. Lian).

https://doi.org/10.1016/j.tust.2019.103061
Received 20 February 2019; Received in revised form 19 April 2019; Accepted 23 July 2019

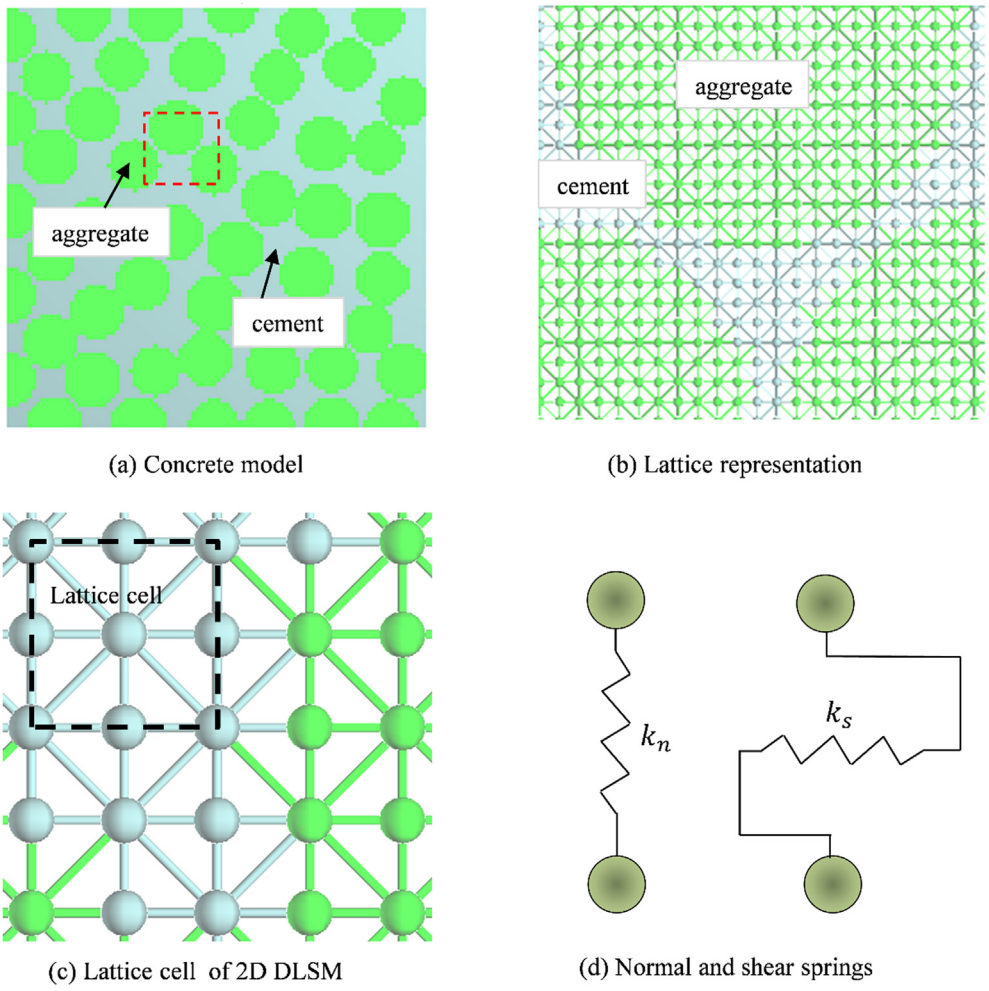

Fig. 1. Basic principles and components of concrete characterized by the 2D DLSM.

necessary to introduce the shear transfer coefficient and keep the cracking direction and the main stress-strain direction consistent (Rots, 1991). The fracture mechanics-based method (Calayir and Karaton, 2005, Wang et al., 2017a, Huang, 2018) is a discrete crack method for solving crack propagation. This method can explicitly represent the discontinuous displacement field but must track the evolution of individual cracks (Wang et al., 2017a). Overall, when these methods are implemented with the finite element method (FEM), they usually exhibit problems related to the complex re-meshing and inability to capture the stress singularity at the crack tip (Huang, 2018). The extended finite element method (XFEM) (Belytschko and Black 1999, Daux et al., 2000; Stolarska et al., 2001) can solve these problems; however, because of the special integration technology, it is much more computationally intensive than the traditional FEM, and its implementation in 3D is very complicated.

With the development of computer science, in recent years, researchers have paid more attention to discrete numerical methods. These methods have successively demonstrated various advantages in solving crack propagation problems. For example, they can naturally express complicated dynamic cracking patterns, multiple crack intersections and three-dimensional crack propagation (e.g., Jiang et al., 2017). The discrete element method (DEM) is the representative method (Cundall, 1971; Potyondy and Cundall, 2004). The DEM has been used to study the crack propagation in concrete (Haeri et al., 2018), but its parameter selection still poses a problem (Kazerani and Zhao, 2010, Zhao et al., 2019). To solve this issue, Zhao et al. (2011) developed a new discrete method called the distinct lattice spring model (DLSM). In the DLSM, they introduced a multi-body shear spring to solve the Poisson's ratio limitation in the classical Lattice Spring Model (LSM). Because the rotation of each particle is characterized by the deformation of the particle's local cluster, unlike in the DEM, each particle has only half a degree of freedom. Therefore, the DLSM has a higher computational efficiency and is suitable for parallel computing (Zhao et al., 2013; Zhao and Khalili, 2012). The DLSM was originally proposed to solve problems involving the brittle failure of rock (Zhao et al., 2011) and has subsequently been used for dynamic crack propagation (Kazerani et al., 2010; Wang et al., 2017b). The ability of DLSM to solve crack propagation problems has been quantitatively compared with classical fracture mechanics and physical tests (Jiang et al., 2017). Recently, Zhao and Xia (2018) adopted the DLSM to study dynamic self-similar cracks, and the numerical results were consistent with analytical solutions and experimental results. The DLSM has demonstrated some advantages in solving crack propagation problems; however, no work has yet to be performed on the quasi-brittle crack propagation in concrete.

In this work, the ability of the original DLSM to solve quasi-brittle crack propagation in concrete is investigated and further developed. First, the ability of the DLSM to reproduce the experimental results of the three-point bending test of concrete was studied by considering factors such as the geometric non-uniformity, material heterogeneity and micro-mechanical constitutive model. Following this, a new micromechanical constitutive model for quasi-brittle crack propagation is developed for the DLSM by further integration of a well-known cohesive zone model (CZM) for concrete and the brittle constitutive model

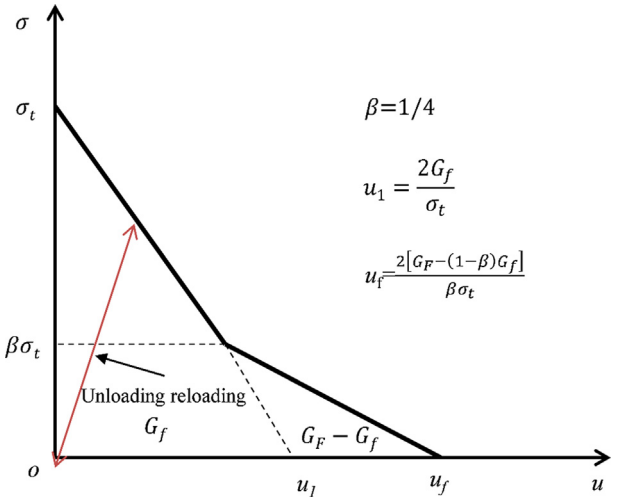

Fig. 2. The bilinear CZM for describing the quasi-brittle cracking of concrete.

of the DLSM. Formulas that describe the relationship between the micromechanical parameters and the macroscopic material parameters are derived and can be used to determine the micromechanical parameters in a more convenient way. The newly developed quasi-brittle constitutive model of the DLSM is further verified against three-point beam bending tests, in which specimens were made of concrete of various grades. Finally, the new constitutive model is further adopted to study the cracking pattern of concrete lining of different grades under various in situ stresses.

2. The DLSM for quasi-brittle crack propagation

This section introduces the extension of the DLSM to solve the quasi-brittle crack propagation in concrete. In this work, an explicit 2D DLSM is adopted, the basic principle and components of which are shown in Fig. 1. The LSM did not attract much attention when it was first developed in 1941. In the 1960s, it captured researchers' interests due to its ability to solve problems on the fracturing of concrete through replacing the spring element with a beam-like element. Unlike the traditional continuum mechanics approaches, the way that the LSM represents concrete is shown in Fig. 1a, in which the aggregate and mortar are explicitly represented by a number of smaller particles that are linked by springs. Nevertheless, the LSM with a beam element still requires an upper bound value of Poisson's ratio, namely, 0.25 for 3D elastic problems and 0.33 for plane strain elastic problems (Zhao et al., 2011, Zhao, 2017). Moreover, the introduction of beam elements would result in the failure constitutive model and micromechanical parameters becoming too complex and difficult to determine. The DLSM was developed to address these problems. It should be mentioned that the DLSM (Zhao et al., 2011) was initially developed for 3D mechanical problems. The DLSM can use lattice models with arbitrary configurations, i.e., both regular and irregular lattices can be used. However, for crack propagation, the 2D DLSM has a higher computing efficiency than the 3D DLSM with the current available computing resources (Jiang and Zhao, 2018). The regular lattice configuration shown in Fig. 1c has been tested and verified comprehensively, and it has been proven to be able to solve linear elastic problems correctly (Jiang and Zhao, 2018). Therefore, this lattice configuration is adopted in this work. As shown in Fig. 1d, in the DLSM, interactions between two particles are represented by a normal spring and a shear spring. The cracking of concrete is well characterized by the progressive failure of these springs.

2.1. The constitutive model

The original constitutive model in the DLSM is a brittle model. Considering the coupling between the normal spring and the shear spring, this constitutive model can be written as

$$f_n = \begin{cases} k_n u_n & , \ u_n < u_n^* \quad \text{and} \quad |u_s| < u_s^* \\ 0 & , \ u_n \geqslant u_n^* \quad \text{or} \quad |u_s| \geqslant u_s^* \end{cases} \tag{1}$$

$$f_s = \begin{cases} k_s u_s & , \ u_n < u_n^* \quad \text{and} \quad |u_s| < u_s^* \\ 0 & , \ u_n \geqslant u_n^* \quad \text{or} \quad |u_s| \geqslant u_s^* \end{cases} \tag{2}$$

where f_n is the normal spring force; k_n is the normal spring stiffness; u_n is the normal spring deformation; f_s is the shear spring force; k_s is the shear spring stiffness; u_s is the shear spring deformation; u_n^* is the ultimate deformation value of the normal spring; u_s^* is the ultimate deformation value of the shear spring; and $|u_s|$ is the absolute deformation value of the shear spring.

This model can be represented as two three-dimensional surfaces. In practice, if only the failure of the normal spring is considered, i.e., $u_s^* = \infty$, this model can be simplified as a two-dimensional curve. The basic principle of CZM for handling crack propagation problems is similar to that of the LSM. Therefore, we will borrow the idea developed for the CZM to solve quasi-brittle crack propagation. Fig. 2 shows the traditional bilinear CZM developed for the quasi-brittle crack propagation in concrete. The model describes the relationship between the crack surface stress and the crack opening displacement. The mathematical expression is written as

$$\sigma(u) = \begin{cases} \sigma_t\left(1 - \frac{u}{u_1}\right) & , \quad u < (1-\beta)u_1 \\ \beta\sigma_t\left(1 - \frac{u-(1-\beta)u_1}{u_f-(1-\beta)u_1}\right) & , \quad (1-\beta)u_1 < u < u_f \\ 0 & , \quad u \geqslant u_f \end{cases} \tag{3}$$

where $\sigma(u)$ is the cohesive stress and u is the opening degree of the crack propagation surface. Its parameters can be fully determined by three material parameters, i.e., the tensile strength of concrete σ_t, fracture energy G_F and initial fracture energy G_f. According to the study of Wittmann et al. (1988), the proportion of the intensity turning point (β) is recommended to be 1/4. Both the tensile strength and fracture energy can be determined from traditional mechanical experiments of the concrete. Two characteristic crack opening values can be determined by the tensile strength and the corresponding fracture energies, i.e., $u_1 = \frac{2G_f}{\sigma_t}$ and $u_f = \frac{2[G_F-(1-\beta)G_f]}{\beta\sigma_t}$. From these equations, it can be seen that the maximum opening is independent of the size of the numerical element and can be treated as a material constant. However, a problem exists for this model: the loading and unloading modulus corresponding to the initial crack opening are infinite (see Fig. 2), which might induce some numerical instability problems. To overcome this shortcoming, it is possible to include an initial elastic stage, called the intrinsic CZM. However, for the FEM or other continuum-based numerical methods (Wu et al., 2018b, a), the intrinsic CZM will cause redundancy among the elastic parameters, i.e., two macroscopic elastic parameters (elastic modulus and Poisson's ratio) and two additional micro-mechanical parameters (normal stiffness and shear stiffness) are needed. This problem also exists in many numerical methods using a similar methodology, e.g., the combined FEM/DEM developed by Munjiza et al. For the DLSM, this problem can be resolved. Fig. 3 shows a new constitutive model developed for quasi-brittle crack propagation in the DLSM. The elastic part is the original brittle constitutive model of the DLSM, and the remaining part is the quasi-brittle CZM, as shown in Fig. 2. The new constitutive model has some interesting features. First, the brittle part is related to the particle size, i.e., the deformation limitation at the peak point is obtained by the following formula:

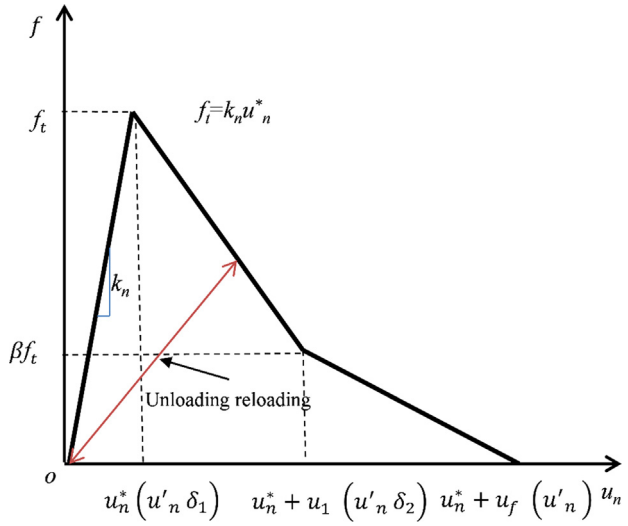

Fig. 3. The new quasi-brittle constitutive model of the DLSM.

$$u_n^* = \gamma\frac{D\sigma_t}{E} \tag{4}$$

where u_n^* is the ultimate deformation value of the normal spring; γ is a correction coefficient of approximately 1, which is suggested to be approximately 0.8 for the nonlinear constitutive model (Li et al., 2019); D is the mean particle size; σ_t is the uniaxial tensile strength; and E is the elastic modulus. The ultimate tensile deformation of the new constitutive model is expressed as

$$u_n' = u_n^* + u_f = \gamma\frac{D\sigma_t}{E} + \frac{2[G_F - (1-\beta)G_f]}{\beta\sigma_t} \tag{5}$$

The peak deformation can be further expressed by a coefficient, which can be related to the ultimate deformation:

$$\delta_1 = \frac{u_n^* + u_f}{u_n'} = \frac{D\gamma\beta\sigma_t^2}{D\gamma\beta\sigma_t^2 + 2[G_F - (1-\beta)G_f]E} \tag{6}$$

The post-peak turning-point deformation can also be represented by another non-dimensional coefficient:

$$\delta_2 = \frac{u_n^* + (1-\beta)u_1}{u_n'} = \frac{\gamma\beta D\sigma_t^2 + 2(1-\beta)\beta G_f E}{\gamma D\beta\sigma_t^2 + 2[G_F - (1-\beta)G_f]E} \tag{7}$$

The damage function is adopted to represent the quasi-brittle constitutive model as

$$f_n = (1 - \max(D^*, D(u_n)))k_n u_n \tag{8}$$

where f_n is the normal spring force, D^* is the maximum history damage of the spring, and $D(u_n)$ is the damage function of current deformation. Formula (8) can characterize the constitutive model of the normal spring by considering the loading and unloading conditions. The damage function of the quasi-brittle constitutive model in the DLSM is further expressed as

$$D(u_n) = \begin{cases} 0 & , \quad u_n < \delta_1 u' \\ 1 + \frac{u_n'\delta_1\beta}{u_n} - \frac{(\delta_2 u_n' - u_n)(1-\beta)\delta_1}{(\delta_2-\delta_1)u_n} & , \quad \delta_1 u' \leqslant u_n < \delta_2 u' \\ 1 - \frac{(u_n' - u_n)\beta\delta_1}{(1-\delta_2)u_n} & , \quad \delta_2 u' \leqslant u_n < u' \\ 1 & , \quad u_n \geqslant u_n' \end{cases} \tag{9}$$

For the shear spring, the same damage function model $D(u_s)$ is adopted. When considering the coupling between the normal spring and the shear spring, the damage function of the spring bond made from these two springs can be further written as

$$D(u_n, u_s) = \max(D(u_n), D(u_s)) \tag{10}$$

The quasi-brittle crack propagation constitutive model in the DLSM represented by Eq. (10) can be graphically plotted as two 3D surfaces. As shown in Fig. 4a, the quasi-brittle constitutive model is tent-like in the normal and shear deformation spaces for the normal spring and the shear spring. However, the damage mechanism of the shear spring is still unclear and will not be considered in this paper. It should be noted that considering the failure of only the normal spring, the DLSM was shown to be able to describe both the Mode-I and mixed mode crack propagation of brittle materials (Jiang et al. 2017). When considering the failure of only the normal spring, Eq. (10) can be further simplified:

$$D(u_n, u_s) = D(u_n) \tag{11}$$

Here, the shear spring force can be obtained by the following equation:

$$f_s = (1 - \max(D^*, D(u_n)))k_s u_s \tag{12}$$

where f_s is the shear spring force, k_s is the shear spring stiffness, and u_s is the shear spring deformation. Fig. 4b shows the two three-dimensional surfaces of the quasi-brittle constitutive model in the DLSM with considering only the normal spring failure. It should be noted that ignoring the shear spring failure does not mean that the shear spring does not break (e.g., the shear spring could break when the normal spring breaks).

2.2. Normal and multi-body shear springs

When the deformation between two particles is given, the corresponding spring force can be obtained with Eqs. (8) and (12). Deformation of the normal spring of the DLSM is consistent with that in the traditional LSM. For example, if the displacements of two particles are given as (u_i, v_i) and (u_j, v_j), the normal deformation of the spring from particle i to particle j can be expressed as

$$u_n = \frac{(u_j - u_i)(x_j - x_i) + (v_j - v_i)(y_j - y_i)}{\sqrt{(x_j - x_i)^2 + (y_j - y_i)^2}} \tag{13}$$

where (x_i, y_i) and (x_j, y_j) are the coordinates corresponding to the two particles, respectively.

For the shear interaction between particles in the DLSM, the concept of the multi-body shear spring was adopted. The basic concept is that the shear deformation between two particles should be calculated by the current deformation states among two particles, described by themselves and a collection of their neighbours, rather than only by the displacements of the two particles. Because multiple particles are involved, the shear spring is called a multi-body shear spring. The necessity and mathematical proof of the multi-body shear spring were demonstrated in detail in the original work of DLSM (Zhao et al., 2011). For the 2D DLSM, when a particle is given, a particle cluster can be formed by the particle and its direct neighbour particles. If a particle location is given as (x,y), the displacement function of the cluster can be approximated by a first-order function:

$$\begin{aligned} u &= a_1 x + b_1 y + c_1 \\ v &= a_2 x + b_2 y + c_2 \end{aligned} \tag{14}$$

The coefficients of the displacement function (a_1, b_1, c_1, a_2, b_2 and c_2) can be obtained by solving a minimum problem of the following quadratic function.

$$\begin{aligned} J_x &= \sum_{j=1}^{n} (u_j - \tilde{u}_j)^2 \\ J_y &= \sum_{j=1}^{n} (v_j - \tilde{v}_j)^2 \end{aligned} \tag{15}$$

where u_j and v_j are the current displacements of the particles and $\tilde{u}_j$ and $\tilde{v}_j$ are the particle displacements corresponding to the displacement approximation function:

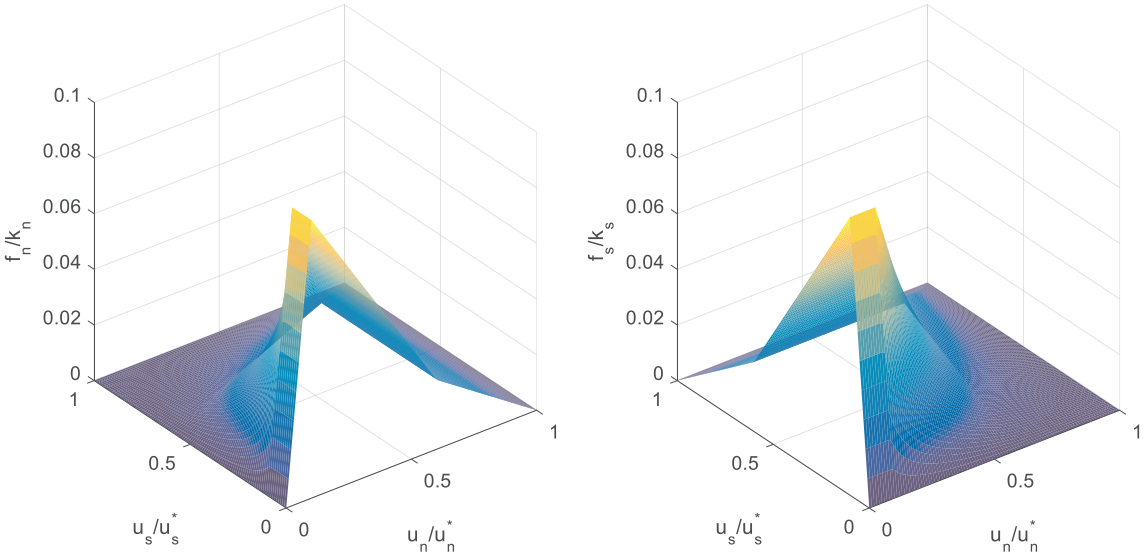

(a) Constitutive model considering both normal and shear springs failure

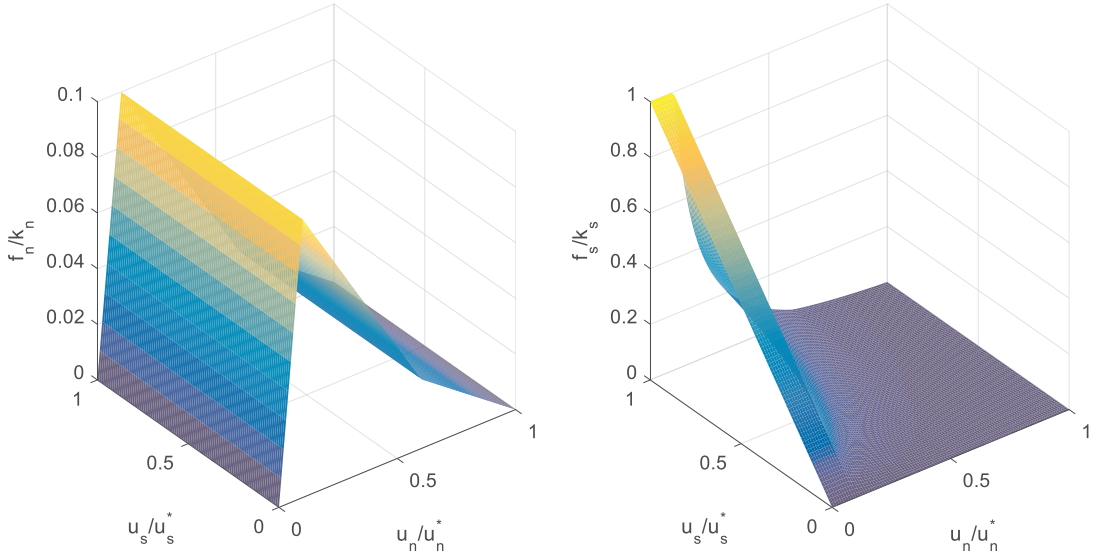

(b) Constitutive model considering only normal failure

Fig. 4. Three-dimensional characterization of the quasi-brittle constitutive model considering the coupling of the normal and shear springs.

$$\tilde{u} = a_1 x + b_1 y + c_1$$
$$\tilde{v} = a_2 x + b_2 y + c_2 \tag{16}$$

Then, the corresponding coefficients can be obtained by the principle of the least square method as

$$(a_1 \;\; b_1 \;\; c_1)^T = (\boldsymbol{A}^T\boldsymbol{A})^{-1}(\boldsymbol{A}^T\boldsymbol{\beta}_1)$$
$$(a_2 \;\; b_2 \;\; c_2)^T = (\boldsymbol{A}^T\boldsymbol{A})^{-1}(\boldsymbol{A}^T\boldsymbol{\beta}_2) \tag{17}$$

where

$$\boldsymbol{A} = \begin{bmatrix} x_1 & y_1 & 1 \\ x_2 & y_2 & 1 \\ \vdots & \vdots & \vdots \\ x_n & y_n & 1 \end{bmatrix}, \boldsymbol{\beta}_1 = \begin{bmatrix} u_1 \\ u_2 \\ \vdots \\ u_n \end{bmatrix}, \boldsymbol{\beta}_2 = \begin{bmatrix} v_1 \\ v_2 \\ \vdots \\ v_n \end{bmatrix} \tag{18}$$

The local strain of the particle cluster can be given as

$$\begin{bmatrix} \varepsilon_{xx} \\ \varepsilon_{yy} \\ \varepsilon_{xy} \end{bmatrix} = \begin{bmatrix} a_1 \\ b_2 \\ (b_1 + a_2)/2 \end{bmatrix} \tag{19}$$

Supposing that the local strains corresponding to two particles linked to a shear spring are $(\varepsilon_{xx,i} \;\; \varepsilon_{yy,i} \;\; \varepsilon_{xy,i})^T$ and $(\varepsilon_{xx,j} \;\; \varepsilon_{yy,j} \;\; \varepsilon_{xy,j})^T$, respectively; the strain state of the shear spring can be obtained as

$$\begin{pmatrix} \varepsilon_{xx,bond} & \varepsilon_{xy,bond} \\ \varepsilon_{xy,bond} & \varepsilon_{yy,bond} \end{pmatrix} = \begin{pmatrix} \frac{\varepsilon_{xx,i} + \varepsilon_{xx,j}}{2} & \frac{\varepsilon_{xy,i} + \varepsilon_{xy,j}}{2} \\ \frac{\varepsilon_{xy,i} + \varepsilon_{xy,j}}{2} & \frac{\varepsilon_{yy,i} + \varepsilon_{yy,j}}{2} \end{pmatrix} \tag{20}$$

The corresponding multi-body shear deformation (vector) can be expressed as

$$\begin{pmatrix} u_s \\ v_s \end{pmatrix} = \begin{pmatrix} \varepsilon_{xx,bond} & \varepsilon_{xy,bond} \\ \varepsilon_{xy,bond} & \varepsilon_{yy,bond} \end{pmatrix} \begin{pmatrix} n_x \\ n_y \end{pmatrix} - \left(\left(\begin{pmatrix} \varepsilon_{xx,bond} & \varepsilon_{xy,bond} \\ \varepsilon_{xy,bond} & \varepsilon_{yy,bond} \end{pmatrix} \begin{pmatrix} n_x \\ n_y \end{pmatrix} \right)^T \begin{pmatrix} n_x \\ n_y \end{pmatrix} \right) \begin{pmatrix} n_x \\ n_y \end{pmatrix} \tag{21}$$

where

$$n_x = \frac{x_j - x_i}{\sqrt{(x_j - x_i)^2 + (y_j - y_i)^2}},\ n_y = \frac{y_j - y_i}{\sqrt{(x_j - x_i)^2 + (y_j - y_i)^2}}$$

The corresponding force (vector) of a multi-body shear spring considering the quasi-brittle crack propagation in concrete can be further characterized as:

$$\begin{pmatrix} f_{us} \\ f_{vs} \end{pmatrix} = (1 - \max(D^*, D(u_n)))k_s \begin{pmatrix} u_s \\ v_s \end{pmatrix} \tag{22}$$

The normal spring force (vector) considering quasi-brittle crack propagation is demonstrated as:

$$\begin{pmatrix} f_{un} \\ f_{vn} \end{pmatrix} = (1 - \max(D^*, D(u_n)))k_n u_n \begin{pmatrix} n_x \\ n_y \end{pmatrix} \tag{23}$$

2.3. Solution procedure

This paper intends to use the explicit solution, not the implicit 2D DLSM (Zhao et al., 2012). The system equations are solved using Newton's second law. To obtain the quasi-static solution, local damping is used, and the specific velocity iteration formula is given as follows.

$$\begin{cases} \dot{u}_i^{\left(t+\frac{\Delta t}{2}\right)} = \dot{u}_i^{\left(t-\frac{\Delta t}{2}\right)} + \left\{\sum f_{x,i}^{(t)} - \alpha \left|\sum f_{x,i}^{(t)}\right| \mathrm{sgn}\left(\dot{u}_i^{\left(t-\frac{\Delta t}{2}\right)}\right)\right\}\frac{\Delta t}{m_p} \\ \dot{v}_i^{\left(t+\frac{\Delta t}{2}\right)} = \dot{v}_i^{\left(t-\frac{\Delta t}{2}\right)} + \left\{\sum f_{y,i}^{(t)} - \alpha \left|\sum f_{y,i}^{(t)}\right| \mathrm{sgn}\left(\dot{v}_i^{\left(t-\frac{\Delta t}{2}\right)}\right)\right\}\frac{\Delta t}{m_p} \end{cases} \tag{24}$$

where $\dot{u}_i^{\left(t+\frac{\Delta t}{2}\right)}$ and $\dot{v}_i^{\left(t+\frac{\Delta t}{2}\right)}$ are the velocities of particle i in the x and y directions at $t + \frac{\Delta t}{2}$, $\dot{u}_i^{\left(t-\frac{\Delta t}{2}\right)}$ and $\dot{v}_i^{\left(t-\frac{\Delta t}{2}\right)}$ are the velocities of particle i in the x and y directions at $t - \frac{\Delta t}{2}$, $\sum f_{x,i}^{(t)}$ and $\sum f_{y,i}^{(t)}$ are the components of the unbalanced force of the particle in the x and y directions at t, Δt is the time step, α is the damping coefficient and is set as 0.6 in this paper, and $\mathrm{sgn}(\cdot)$ is a sign function given by the following formula:

$$\mathrm{sgn}(x) = \begin{cases} -1, x < 0 \\ 0\ , x = 0 \\ 1\ , x > 0 \end{cases} \tag{25}$$

As the particle velocity updates, the corresponding particle displacement can be updated as

$$\begin{cases} u_i^{(t+\Delta t)} = u_i^{(t)} + \dot{u}_i^{\left(t+\frac{\Delta t}{2}\right)}\Delta t \\ v_i^{(t+\Delta t)} = v_i^{(t)} + \dot{v}_i^{\left(t+\frac{\Delta t}{2}\right)}\Delta t \end{cases} \tag{26}$$

2.4. Parameter selection

Unlike the traditional DEM, there is no calibration required in the DLSM. For the 2D DLSM, the spring stiffness between two particles can be given by the following formula for the plane stress problem.

$$k_n = \left(\frac{E_i}{\alpha^{2D}(1 - \upsilon_i)} + \frac{E_j}{\alpha^{2D}(1 - \upsilon_j)}\right) \tag{27}$$

$$k_s = \left(\frac{(1 - 3\upsilon_i)E_i}{\alpha^{2D}(1 - \upsilon_i^2)} + \frac{(1 - 3\upsilon_j)E_j}{\alpha^{2D}(1 - \upsilon_j^2)}\right) \tag{28}$$

Similarly, for the plane strain problem,

$$k_n = \left(\frac{E_i}{\alpha^{2D}(1 - \upsilon_i)(1 - 2\upsilon_i)} + \frac{E_j}{\alpha^{2D}(1 - \upsilon_j)(1 - 2\upsilon_j)}\right) \tag{29}$$

$$k_s = \left(\frac{3(1 - 4\upsilon_i)E_i}{2\alpha^{2D}(1 + \upsilon_i)(1 - 2\upsilon_i)} + \frac{3(1 - 4\upsilon_j)E_j}{2\alpha^{2D}(1 + \upsilon_j)(1 - 2\upsilon_j)}\right) \tag{30}$$

where E_i and E_j are the material elastic modulus corresponding to the two particles, υ_i and υ_j are the Poisson's ratios of particles i and j, and α^{2D} is the geometric coefficient of the lattice model and is given by the following equation:

$$\alpha^{2D} = \frac{\sum l_i^2}{A\Delta} \tag{31}$$

where l_i is the length of the i_{th} bond, A is the representative area of the lattice model, and Δ is the unit thickness of the lattice model in the third dimension.

The derivations of these equations are based on the hyperelasticity analysis principle and the strain energy equivalence principle for the lattice model and the corresponding continuum model. The derivation and verification were demonstrated in detail in the original work on the DLSM (Zhao et al., 2011). Compared with the original DLSM, the DLSM with a quasi-brittle constitutive model includes two additional non-dimensional parameters δ_1 and δ_2 as well as the maximum tensile deformation u_n'. Following the suggestion provided by Wittmann et al. (1988) for the cohesive model shown in Fig. 2, the relationship between the initial fracture energy and the fracture energy can be estimated as

$$G_F = \xi 2.5 G_f \tag{32}$$

For concrete, ξ is approximately 1.0. By substituting Eq. (32) into Eq. (5) and setting β to 0.25, the equation of the maximum normal deformation can be given as follows:

$$u_n' = \gamma\frac{D\vartheta\sigma_t}{E} + \frac{2(16G_F - 3\xi)G_F}{4\vartheta\sigma_t} \tag{33}$$

The corresponding two non-dimensional parameters can be further simplified as

$$\delta_1 = \frac{4D\gamma(\vartheta\sigma_t)^2}{4D\gamma(\vartheta\sigma_t)^2 + 2(16 - 3\xi)G_F E} \tag{34}$$

and

$$\delta_2 = \frac{8\gamma D(\vartheta\sigma_t)^2 + 3\xi G_F E}{8\gamma D(\vartheta\sigma_t)^2 + (64 - 12\xi)G_F E} \tag{35}$$

When the particle size and fracture energy for a concrete are given, the corresponding parameters of the quasi-brittle constitutive model can be determined by using these equations. There are two non-dimensional parameters ϑ and ξ to further adjust the numerical responses. The purpose of introducing these adjusting parameters is to increase the flexibility of the parameter selection of the DLSM. Eqs. (33)–(35) can give a good estimation of the micromechanical parameters; however, an actual numerical simulation in practice might be different from the target experimental results. In this case, it is more convenient to adjust these dimensionless parameters, which are approximately one. Here, the role of ϑ is to increase the microscopic tensile strength by a factor. Taking the mesoscopic tensile strength greater than the macroscopic tensile strength is commonly used in discrete numerical methods. From Eqs. (33)–(35), it can be seen that when the fracture energy is zero, the new constitutive model will simplify to the brittle constitutive model in the original DLSM (Zhao et al., 2011). To consider the material heterogonous, we use the single-parameter Weibull distribution function to assign the maximum normal deformation. This specific distribution function is as follows:

$$f(\varsigma) = m\varsigma^{m-1}e^{-\varsigma^m} \tag{36}$$

where ς is a random number that satisfies the single-parameter Weibull distribution function and m is a coefficient that controls the shape of the distribution function. The larger m is, the more uniform and closer to 1 the distribution of the random number ς (Tang et al., 2015; Xu et al., 2013; Wang et al., 2012; Zhu et al., 2002). A random number is generated for each spring bond, and the corresponding maximum spring deformation considering the material heterogeneous is given as

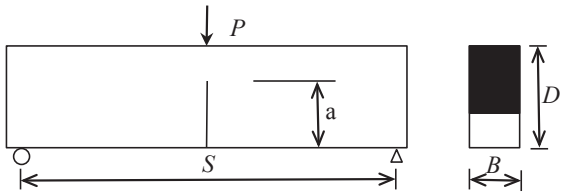

(a) Geometry of the specimen

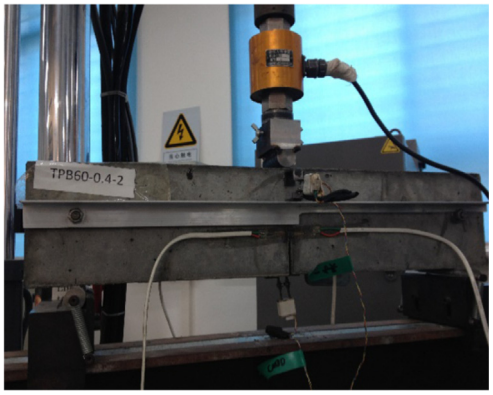

(b) Experimental step

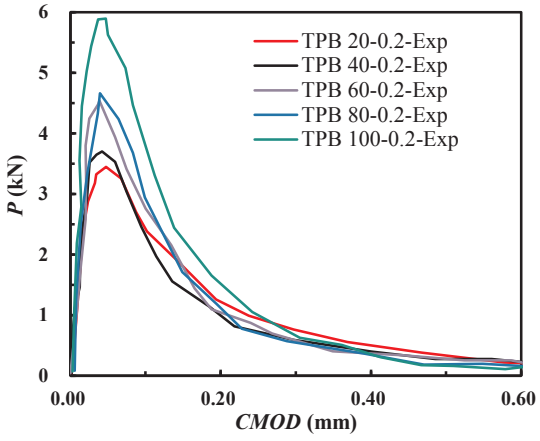

(c) CMOD versus loading force

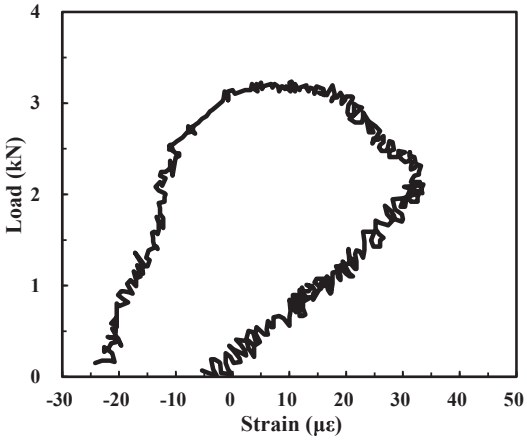

(d) Strain versus loading force

Fig. 5. The experimental setup and typical result of the three-point bending experiment for quasi-brittle crack propagation in concrete (Dong et al., 2016).

$$u'_{n,i} = \varsigma u'_n \tag{37}$$

In an actual simulation, the parameter selection can start by setting both the non-dimensional parameters ϑ and ξ as 1. Then, the simulation results can be compared with the target experimental values. The difference between the numerical results and the experimental results is minimized by adjusting these non-dimensional parameters. Specific examples will be described in the following sections.

3. Quasi-brittle cracking of concrete using the DLSM

In this section, the DLSM is tested and compared with the three-point bending experimental results discussed in Dong et al. (2016) (the specimen's geometrical information can be seen in Fig. 5a), in which the cracking data of concretes with different grades were recorded in detail, especially the quasi-brittle crack propagation data recorded by strain gauges attached at the crack tip (see Fig. 5b). In addition to the typical curve of crack mouth opening displacement (CMOD) versus loading (see Fig. 5c), the strain versus loading curve (Fig. 5d) was also reported and can be used to obtain the loadings at crack initiation and propagation, which is an effective way to describe the crack propagation of the quasi-brittle material. The material parameters of the concrete were recorded in detail as well. Table 1 lists the parameters of the concretes with different grades; these parameters can be used to obtain the micromechanical parameters of the DLSM using Eqs. (33)–(35). Fig. 6 shows the computational model of the DLSM for the three-point bending experiment, in which the dimensions of the model are identical to those in the literature (see Fig. 5a). The boundary conditions are set to allow one end to roll, while the other one is fixed (see Fig. 6). A downward velocity load is applied to the middle of the upper surface of the beam (see Fig. 6). Considering the numerical stability and computational cost, the loading velocity is taken as 1 mm/s. In this work, the time step for the three-point bending numerical experiment is 1×10^{-7}s. The deformation of each iteration is approximately 0.1 nm, which can ensure that the numerical results reflect the quasi-static state. Two measuring points are used to record the histories of the horizontal displacement of the crack surface; this information can be used to obtain the CMOD.

Table 1
The macroscopic parameters of the concretes with different grades (data from Dong et al., 2016).

Concrete	Elastic modulus E (GPa)	Poisson's ratio* υ	Density* ρ	Tensile strength σ_t (MPa)	Fracture Energy G_F (N/m)
C20	29.9	0.2	2450	3.05	127.9
C40	32.2	0.2	2450	3.74	130.6
C60	35.7	0.2	2450	4.43	122.4
C80	38.1	0.2	2450	5.01	141.0
C100	41.4	0.2	2450	5.71	138.0

* Refers to the parameters not provided in the original literature; the classical value is used instead.

$$CMOD(t) = u_{right}(t) - u_{left}(t) \tag{38}$$

To be consistent with the strain gauge recording in the physical experiment, a measuring point is placed 10 mm away from the crack tip in the computational model (see Fig. 6) to record the time history of the

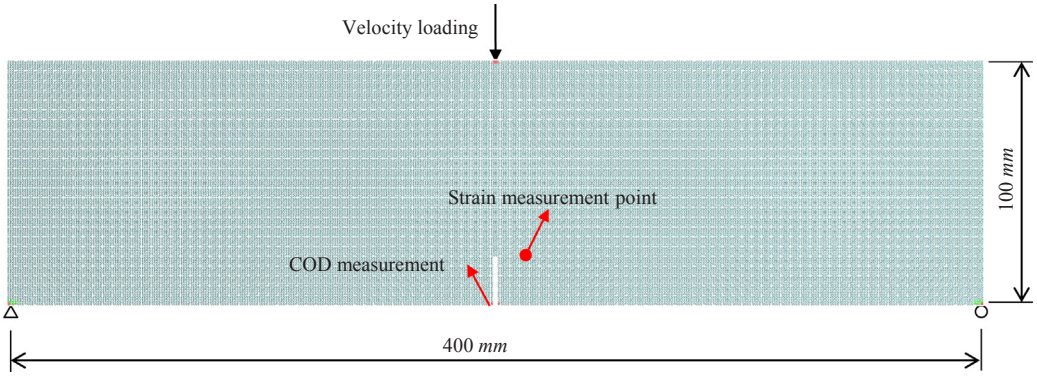

Fig. 6. The computational model and boundary condition settings for the three-point bending experiment of concrete by using the DLSM.

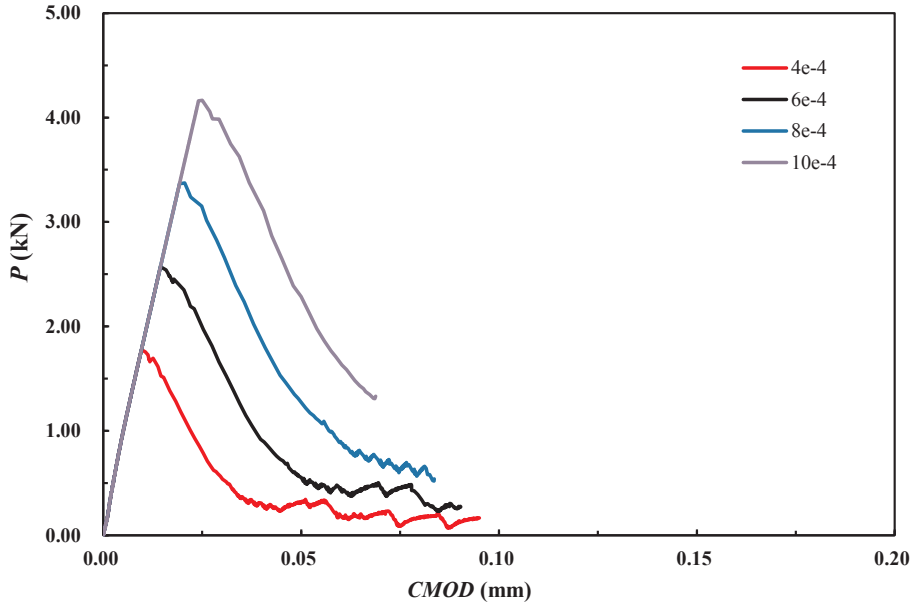

(a) CMOD versus loading force

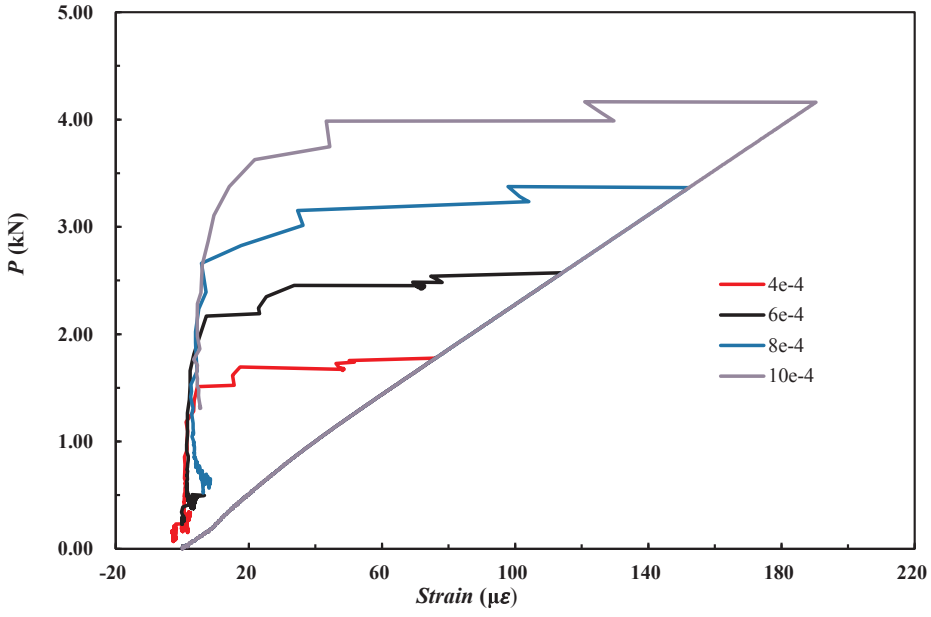

(b) Strain versus loading force

Fig. 7. The numerical simulation results of the original DLSM only considering the brittle constitutive model (unit in mm).

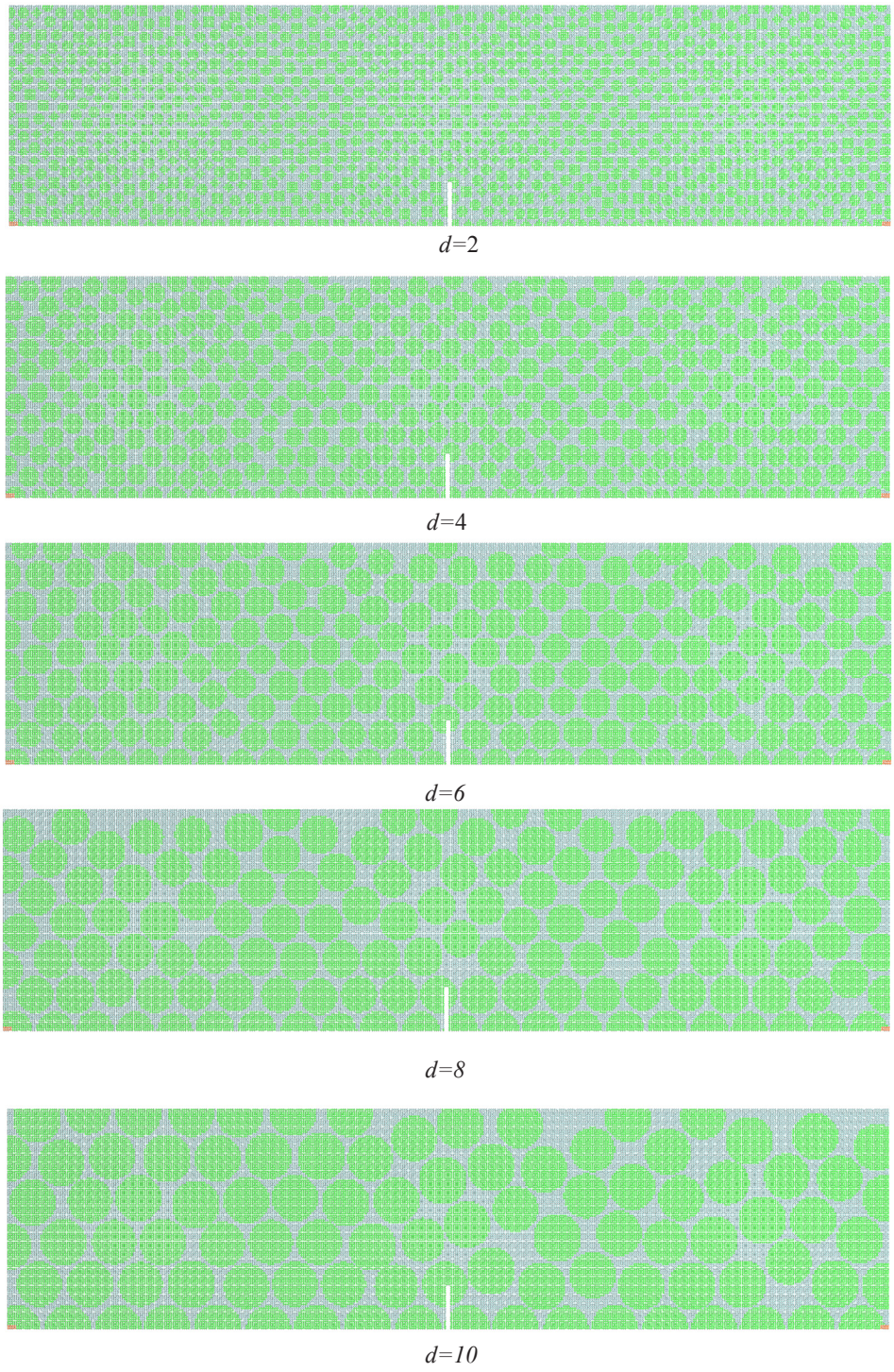

Fig. 8. Computational models with geometric non-uniformity, considering different aggregate/grain sizes (unit in mm).

horizontal strain. Additionally, the time histories of the loading displacement and reaction force are simultaneously recorded with the velocity boundary condition. In this way, the numerical simulation can obtain results consistent with the corresponding physical experiment.

3.1. Brittle constitutive model

In this section, the original DLSM with the brittle constitutive model is first used to simulate the three-point beam bending test using grade C20 concrete. The corresponding material parameters, e.g., elastic modulus and Poisson's ratio, are shown in Table 1. The brittle constitutive model has only one failure parameter u_n', which is evaluated at 4e − 4 mm, 6e − 4 mm, 8e − 4 mm and 10e − 4 mm. Fig. 7 shows the influence of this failure parameter on the numerical simulation results. The maximum loading force can be obtained from the curve of the relationship between the CMOD and the loading force (see Fig. 7a). A significant linear positive correlation was observed between the maximum loading force and the failure parameter u_n'. However, these curves predicted by the DLSM have a distinct linear portion before peaking and cannot accurately reproduce the pre-peak nonlinear hardening curve as observed in the experiment (see Fig. 5c). For the post-peak portion, although only the brittle constitutive model is used,

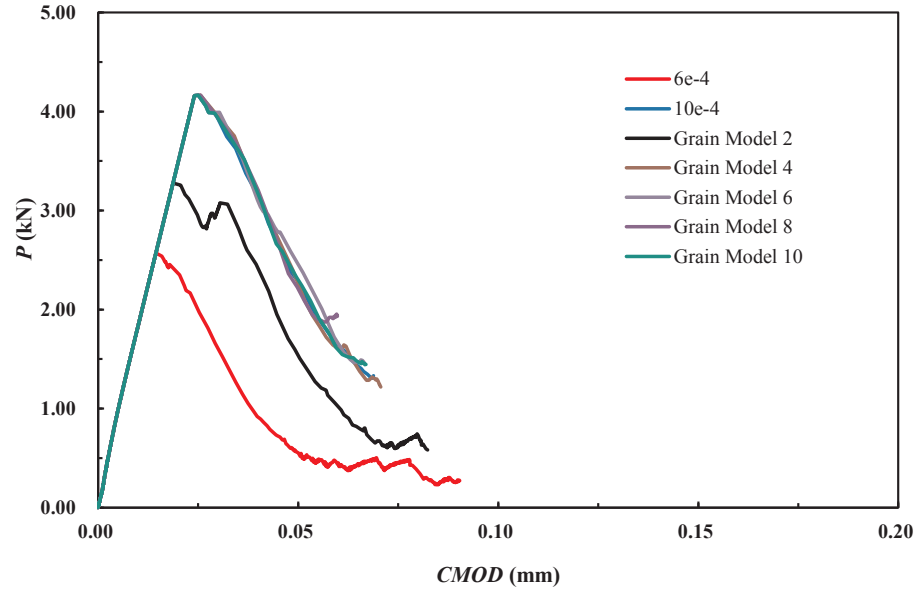

(a) CMOD versus loading force

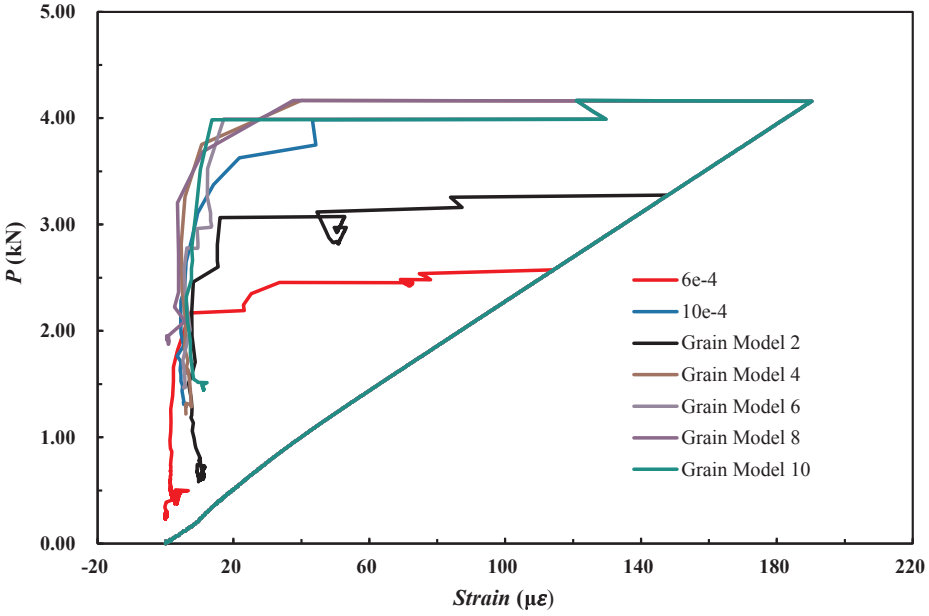

(b) Strain versus loading force

Fig. 9. Numerical simulation results of the DLSM considering the geometric non-uniformity (unit in mm).

the post-peak portion of the CMOD and loading force curve shows a certain slope with softening, rather than exhibiting a brittle drop. This post-peak softening morphology should be related to the loading setting of the three-point bending test. Fig. 7b shows the strain and loading force curves. Unlike the typical dome-shaped curve observed in the physical experiment results, there is no typical distinguishing feature between the crack initiation loading and crack propagation loading in the numerical simulation results, as shown in Fig. 5d. Therefore, it is concluded that the original DLSM with a brittle constitutive model cannot correctly characterize the cracking behaviour of concrete. A homogenous model is adopted in this section. The influence of the geometric non-uniformity will be investigated in the following section.

3.2. Geometric non-uniformity

This section will explore the influence of geometric non-uniformity on the original DLSM when solving quasi-brittle crack propagation problems. Fig. 8 shows the computational models considering the geometric non-uniform distribution of the aggregate and mortar. The elastic parameters of the aggregate are consistent with those of the mortar, but their failure parameters are different. Different aggregate sizes, i.e., 2 mm, 4 mm, 6 mm, 8 mm and 10 mm, are used to generate these models (see Fig. 8). The failure parameter u_n' of the aggregate is set to 10e − 4 mm, and that of the mortar is set to 6e − 4 mm. The simulation results are shown in Fig. 9 with the results of homogenous models in which the material parameters were set to those of the mortar and the aggregate, respectively. Fig. 9a shows the curve of CMOD versus loading force. The aggregate size has a certain influence on the numerical results. For a model with larger aggregate diameter, the simulation results are closer to the results of the homogenous model with the aggregate's material properties, whereas for a model with a small aggregate size, the results are between the results of homogenous

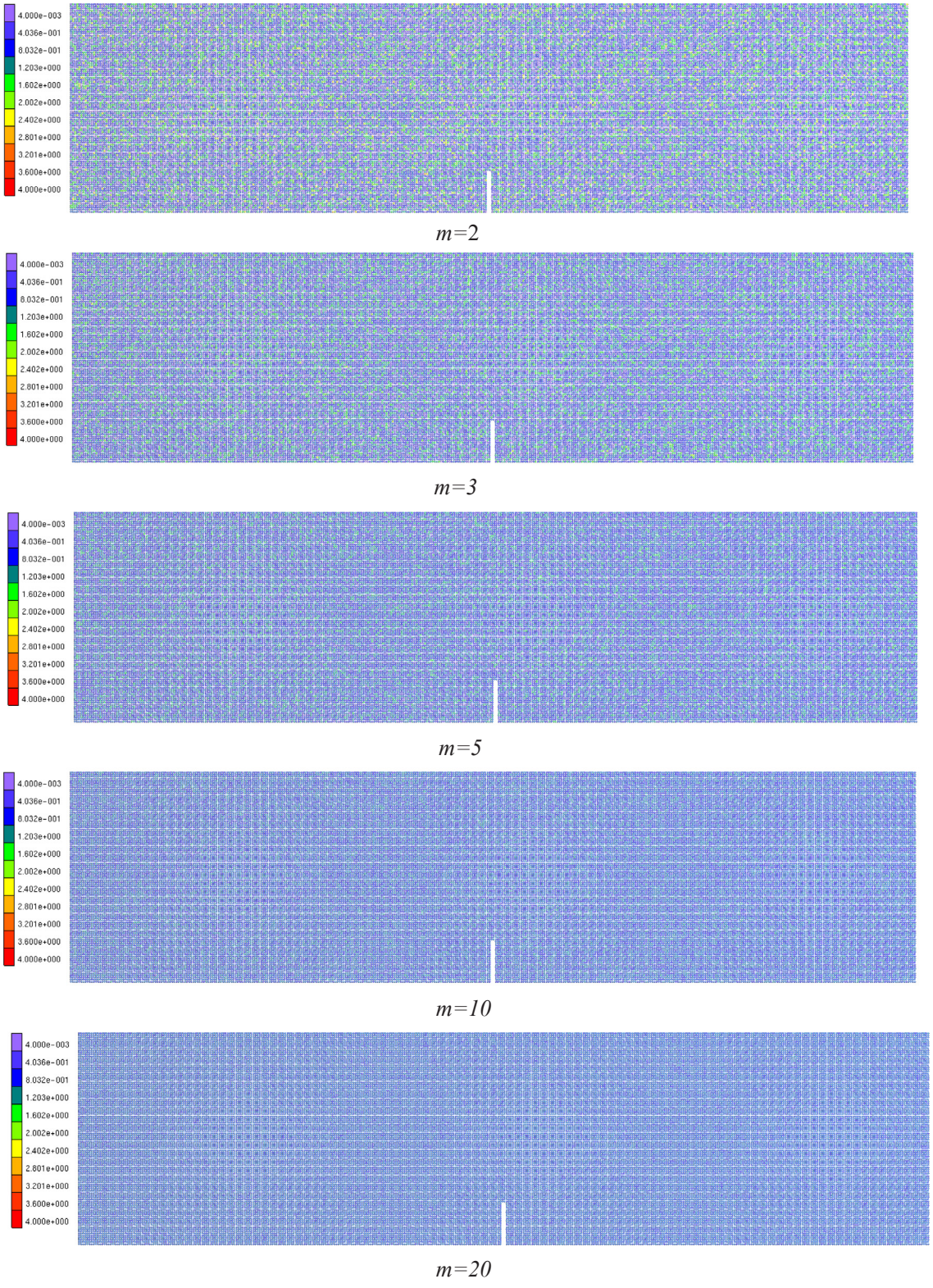

Fig. 10. DLSM computational models considering the material heterogeneity.

models with the material properties of aggregate and mortar, respectively. There is some disturbance in the pre-peak and post-peak portions of the simulation results. However, there is no large difference from the homogeneous model in terms of predicting the nonlinear pre-peak shape of the CMOD versus loading force curve and the dome-shaped curve of the strain versus loading force curve. Therefore, it is impossible to reproduce the physical experimental observations merely by including geometric non-uniformity in the original DLSM. The zigzag phenomenon of the strain versus loading force curves as shown in Fig. 9b should result from the suddenly released strain energy during the fracturing process modelled by the brittle constitutive model.

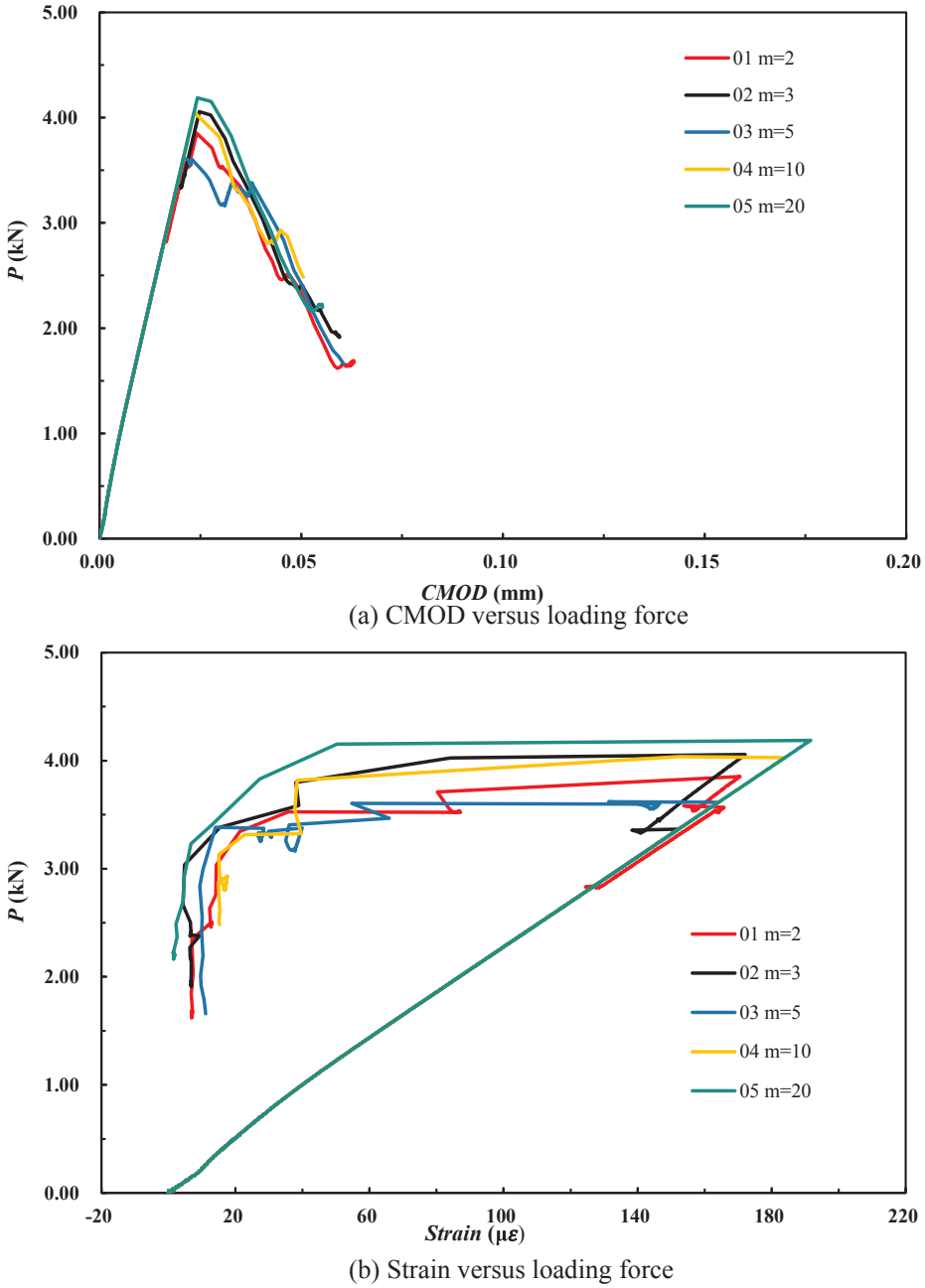

Fig. 11. Numerical results of the DLSM with different material heterogeneities.

Table 2
Micro-mechanical parameters of the quasi-brittle constitutive model for C20 concrete.

Index	D (mm)	ϑ*	ξ*	u_n' (mm)	δ_1	δ_2
1	1	1.0	1.0	0.2019	0.0004	0.1075
2	1	1.0	0.5	0.1154	0.0007	0.3754
3	1	1.5	0.5	0.0770	0.0016	0.3760

* The values need to be calibrated.

3.3. Material heterogeneity

Representing material heterogeneity by using a Weibull distribution function is a classical method to address the realistic fracturing of rock and concrete (Tang et al., 2015). As shown in Fig. 10, different computational models are generated by assigning the random distribution coefficient ς using the single parameter Weibull distribution function with different m values. Fig. 11 shows the numerical results. The larger the m value is, the greater the homogeneity of the computational model and the closer the numerical results to the corresponding results of the homogenous model.

Fig. 11a shows the CMOD and loading force curves. As the m value increases, the corresponding peak loading increases. There is little disturbance and nonlinearity in the pre-peak portion of the results of the computational model with a smaller m value (refers to a greater heterogeneity). However, this portion of the curve is still far from the smooth nonlinear curve observed in the physical experiment. For the post-peak portion of the curve, the material heterogeneity causes it to be flatter and closer to the experimental observations, but a difference still exists. For the strain and loading force curves, the influence of the m value is reflected in the disturbance at the dome and a small disturbance in the front part of the crack initiation loading, but

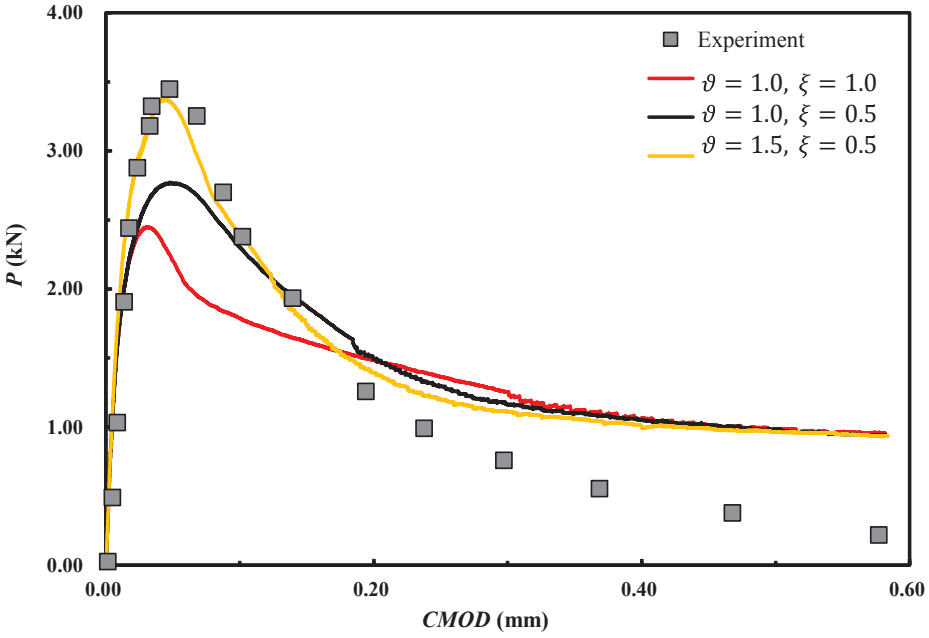

(a) CMOD versus loading force

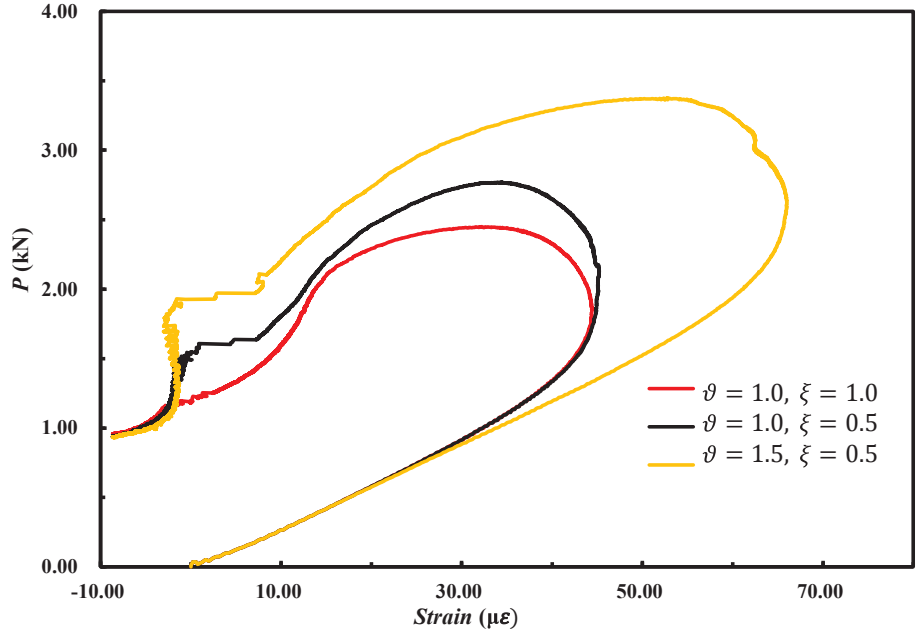

(b) Strain versus loading force

Fig. 12. Numerical simulation results of the DLSM with a new quasi-brittle constitutive model.

Table 3
Micro-mechanical parameters of the quasi-brittle constitutive model of the concretes with different grades.

Concrete	u_n' (mm)	δ_1	δ_2
C40	0.0639	0.0021	0.3763
C60	0.0655	0.0023	0.3764
C80	0.0473	0.0033	0.3771
C100	0.0469	0.0035	0.3772

morphology consistent with the physical experimental observation still cannot successfully be reproduced.

3.4. Quasi-brittle constitutive model

In this section, the new quasi-brittle constitutive model is used to reproduce the experimental results of the C20 concrete specimen. The micromechanical parameters, the maximum normal deformation and two non-dimensional coefficients are calculated using Equations (33)–(35) and are listed in Table 2, in which the two non-dimensional adjusting parameters, ϑ and ξ, are set to different values. From Table 2, it can be seen that the ratio of the post-peak portion to the pre-peak portion of the corresponding micromechanical constitutive model is very high. Therefore, the main part of the curve is still the post-peak

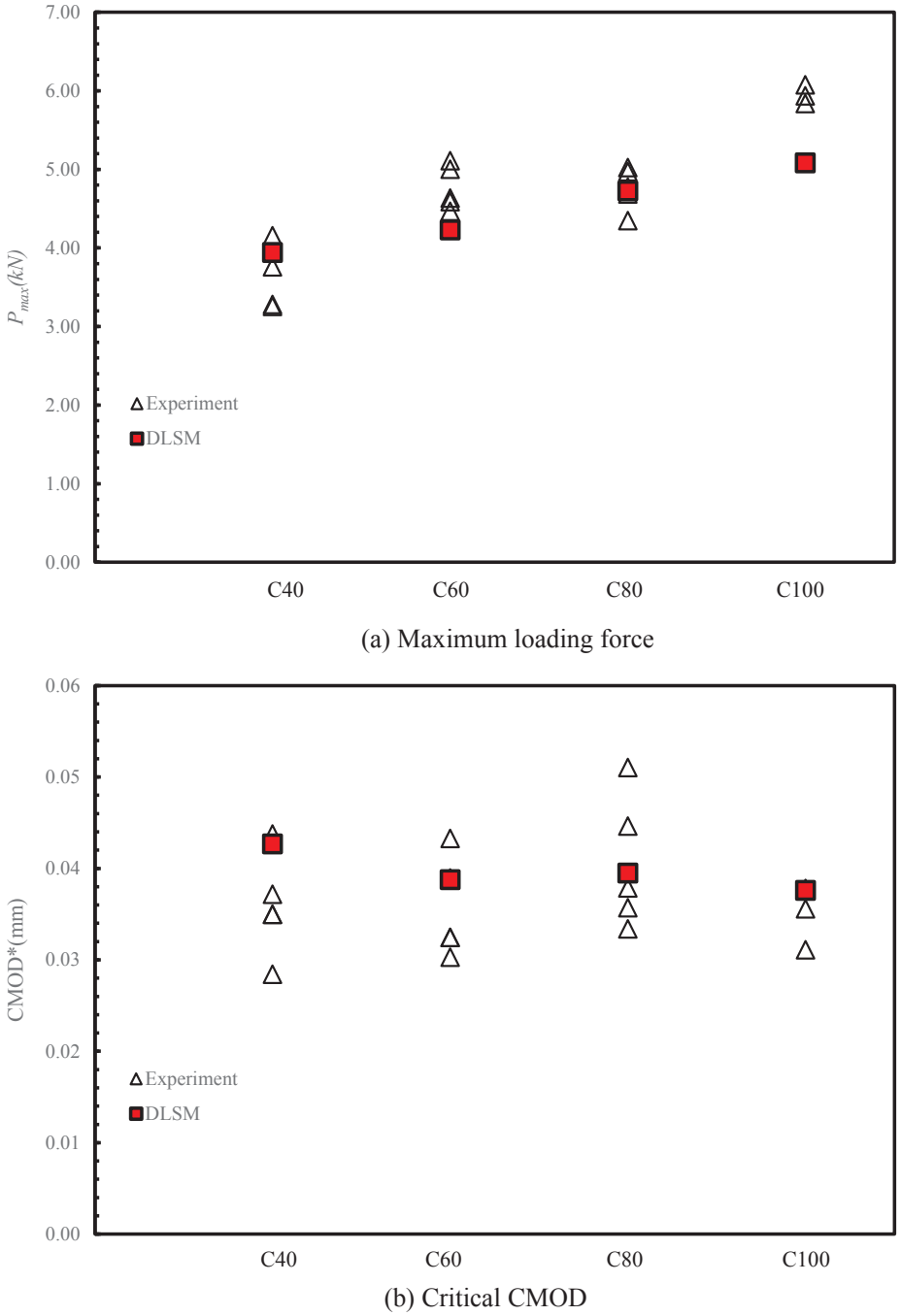

Fig. 13. Comparison between the prediction of the new constitutive model and the corresponding experimental results for concretes with different grades.

portion, and the influence of the elastic portion on the fracture energy can be ignored. When the particle size is large, the elastic portion energy would be large; however, it still needs to be ignored to make the DLSM particle size insensitive for the quasi-brittle cracking.

Fig. 12a shows the CMOD versus loading curve predicted by the quasi-brittle constitutive model. The nonlinear hardening characteristics of the pre-peak portion are consistent with those of the experimental results. Nevertheless, the numerical peak loading force is low compared to its experimental counterpart. The numerical peak loading force can gradually approach the experimental observed value by adjusting the two non-dimensional parameters ϑ and ξ. Through a number of trials, in this work, the two non-dimensional parameters are found to be $\vartheta = 1.5$ and $\xi = 0.5$. Fig. 12b shows the curve of the strain versus loading force. The dome morphology is well reproduced, and the corresponding crack initiation loading and crack propagation can also be well distinguished. It should be mentioned that no qualitative comparison could be made because Dong et al. (2016) did not provide detailed information on their strain versus loading force curve, e.g., which test it belongs to.

3.5. Verification

In this section, the ability of the DLSM with a new quasi-brittle constitutive model to predict cracking in concrete is further verified. Dong et al. (2016) reported a large number of CMOD versus loading force curves for concrete specimens with different grades. The maximum loading force and the corresponding critical CMOD can be extracted from the literature. These two indicators are used as a

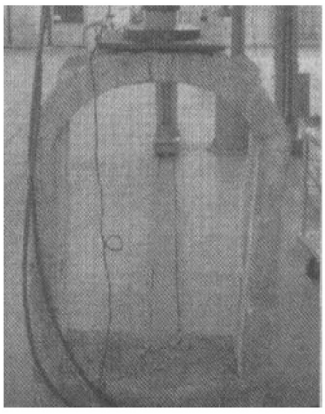

(a) The laboratory experiment of the independent loading of concrete lining (Zhu et al. 2004);

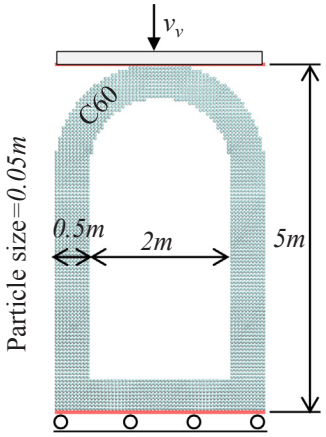

(b) The computational model of the independent loading of concrete lining

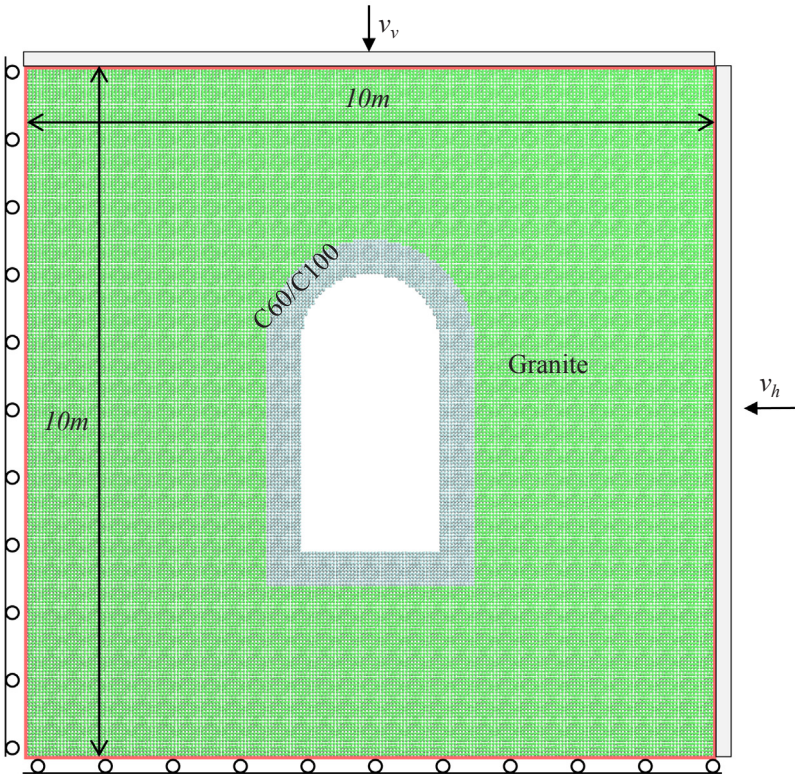

(c) The computational model considering the interaction of the lining and rock mass

Fig. 14. The physical experiment and numerical model of the concrete lining.

Table 4
Micro-mechanical parameters of the concrete lining.

Concrete	D (mm)	u_n' (mm)	δ_1	δ_2
C60	50	0.0664	0.1122	0.4451
C100	50	0.0598	0.1384	0.4615

comparison target to further check the predictive ability of the DLSM. These calibrated ϑ and ξ for the C20 concrete are further adopted for calculating all the micro-mechanical parameters from the three-point bending experiment of concretes with different grades (see Table 3). Therefore, we did not process any calibration in this section. Fig. 13 shows a comparison between the numerical prediction and the corresponding experimental value. Three-point bending testing of concrete specimens was carried out many times for each grade, and the experimental results have a certain dispersion. The material parameters given by Dong et al. (2016) should be based on statistical averages. Therefore, as shown in Fig. 13, the numerical predicted value is approximately the mean value of the experimental results. This further validates the effectiveness of the new quasi-brittle constitutive model developed for the DLSM to predict quasi-brittle crack propagation.

4. Cracking of the concrete lining

Concrete lining is commonly used in underground engineering projects. A concrete lining can provide intuitive security and aesthetics, but if the concrete lining cracks, it could increase the feeling of insecurity. Classical methods for studying concrete lining cracking are analytical and experimental methods. However, analytical methods can

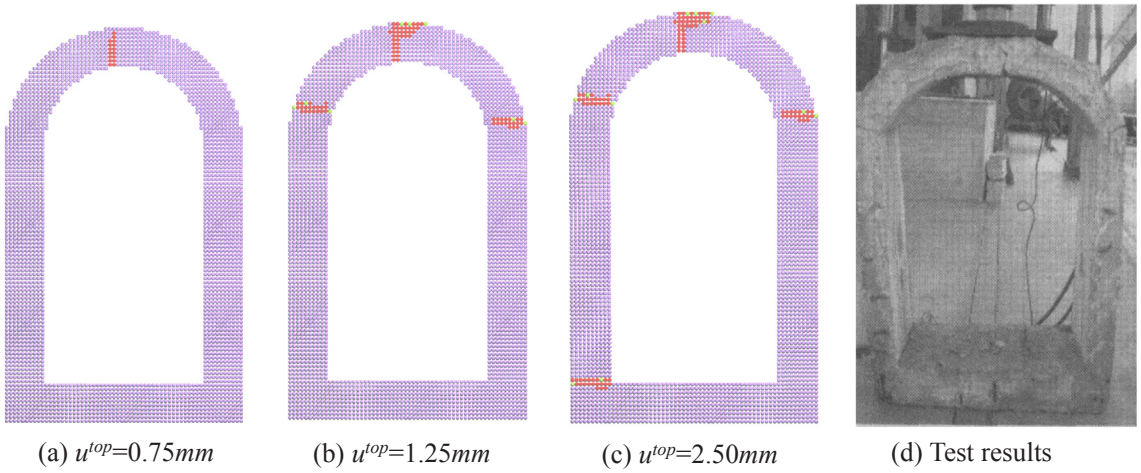

Fig. 15. Failure morphology comparison between the numerical prediction and the experimental result.

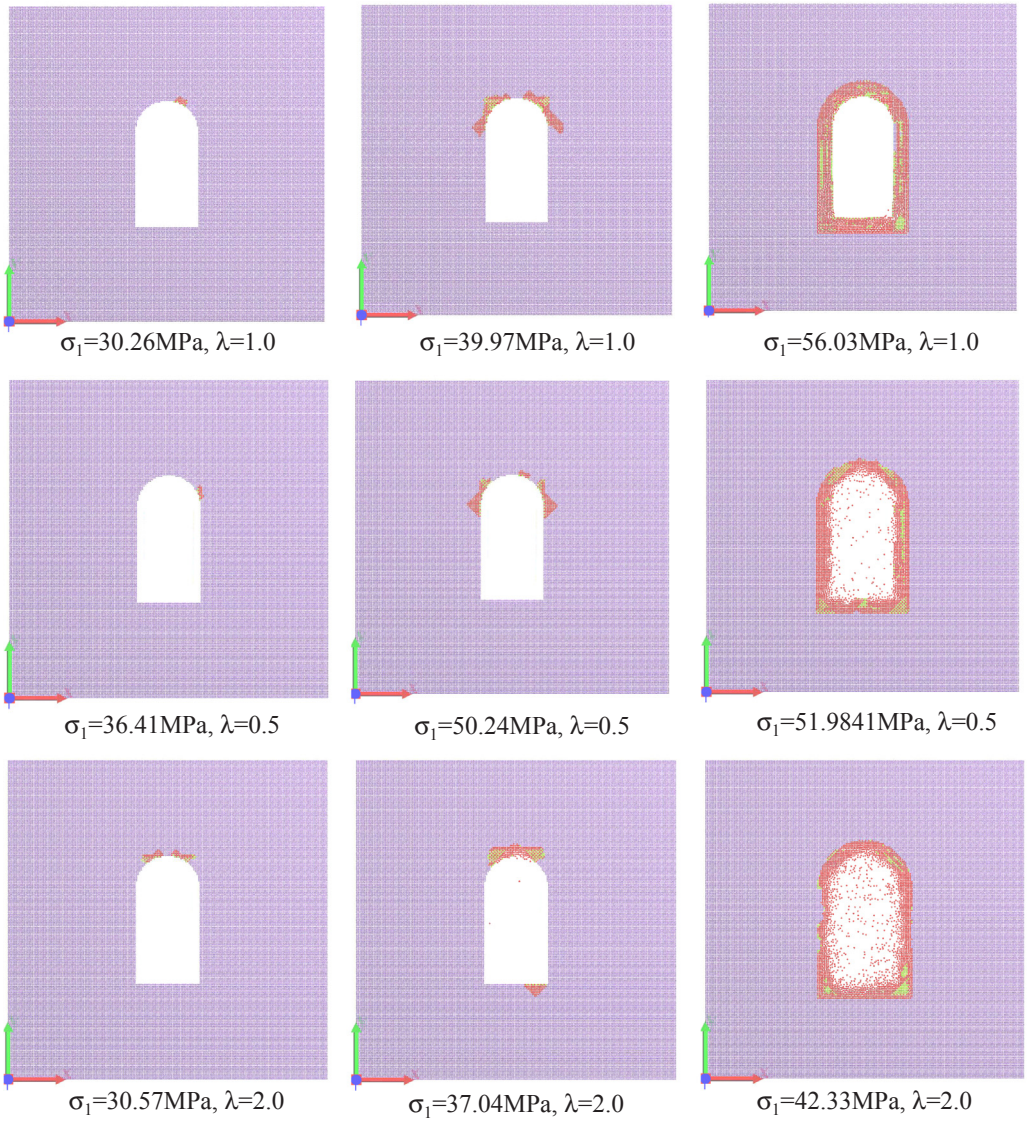

Fig. 16. Failure morphology of the C60 concrete lining under the different vertical and horizontal in situ stresses.

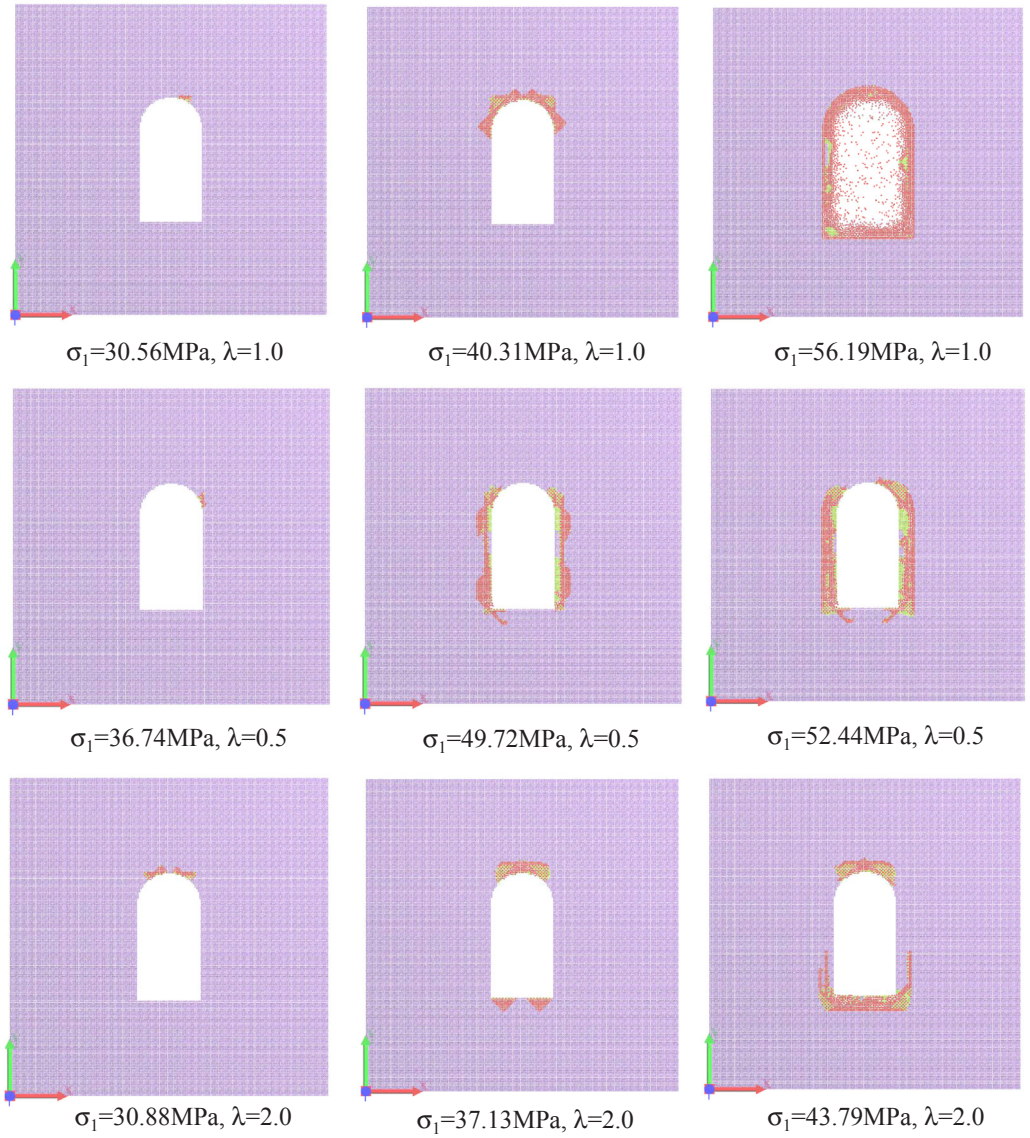

Fig. 17. Failure morphology of the C100 concrete lining under the different vertical and horizontal in situ stresses.

only address concrete lining of an ideal shape with a simple cracking criterion. This approach is incapable of handling the nonlinear cracking behaviour of concrete. A physical test can investigate the cracking morphology of the concrete lining with a complicated shape; however, in addition to the inability to apply a higher confining pressure due to the limits of the testing equipment, the interaction between the rock masses and the concrete lining is difficult to fully consider. Numerical simulation has certain advantages over other methods of study in terms of handling complex geometry and constitutive models. Here, the ability of the new quasi-brittle constitutive model to predict the crack propagation of the concrete lining is checked against experimental testing of the concrete lining, as shown in Fig. 14a (Zhu et al., 2004). The computational model of the loading experiment for the concrete lining is established and shown in Fig. 14b. The computational model dimensions are shown in Fig. 14b, and the selected material is C60 concrete. Since the numerical simulation in this section is quantitative and does not require high precision, a coarser model is used. By setting the particle diameter to a specific value (D = 50 mm), the corresponding micro-mechanical parameters (Table 4) can be obtained by using Eqs. (33)–(35), and the corresponding macroscopic parameters of C60 concrete are shown in Table 1. According to the diagram of the actual physical experiment, the motion fixed in the vertical direction on the lower end face of the model is set as a fixed boundary condition, and a load velocity of 5 mm/s is applied to its upper end face. Zhu et al. (2004) only described the lining failure morphology from the experiment. Fig. 15 shows a comparison between the failure morphology predicted by the DLSM and the corresponding physical observation. The numerical prediction results show that the top of the lining cracked first, then both sides cracked, and finally, the bottom cracked. The crack morphology and sequence of the simulation prediction are in good agreement with those of the physical test. Therefore, the proposed new quasi-brittle crack constitutive model in the DLSM can reasonably simulate the cracking of the concrete lining. On this basis, a computational model considering the interaction between the lining and rock mass is established (Fig. 14c). The material of the rock mass is granite, and the selected material parameters are typical values, i.e., the elastic modulus is 80 GPa, Poisson's ratio is 0.2, and density is 2450 kg/m^3. The granite is assumed to be in an elastic state, and only the failure of concrete is permitted in the numerical simulation. The influence of the in situ stress magnitude and direction on the failure of the concrete lining is studied by a computational model with different horizontal and vertical load velocities (see Fig. 14c). In the simulation, the magnitude of the in situ stress can be obtained by dividing the reaction force on the velocity boundary with the boundary length. For all the

simulations, the maximum in situ stress is controlled to be less than 60 MPa. Therefore, for a C60 concrete lining, the compressive failure of the concrete lining is not considered. The ratio of the horizontal in situ stress to the vertical one is controlled by adjusting the velocities in both directions, and the reference velocity is 5 mm/s. A coefficient λ is used to represent the ratio of the horizontal stress to the vertical stress and is the ratio of the horizontal velocity to the vertical velocity. The λ coefficients of 1.0, 0.5 and 2.0 are investigated in this study. They represent cases of equal, vertical-dominant and horizontal-dominant in situ stresses, respectively. Fig. 16 shows the failure morphologies of the C60 concrete lining under different in situ stresses. When the in situ stress is 30 MPa, the initial crack forms at the top of the lining. The crack continues to propagate with the increase in the in situ stress, which mainly concentrates at the top and bottom of the lining. When the in situ stress increases to 56 MPa, the lining is completely broken. When the λ coefficient is 0.5, the vertical loading is dominant, and the crack initiation position in the concrete lining is different. When the in situ stress of 50 MPais applied, the cracking morphology is widely distributed. As the in situ stress increases to 51 MPa, the lining is completely broken. Therefore, the λ coefficient has a certain influence on the cracking morphology of the concrete lining. A low horizontal in situ stress would have an adverse effect on the cracking of the concrete lining. When the λ coefficient is 2.0, the horizontal loading is dominant, and the crack initiation location in the concrete lining is not considerably different from the first two cases. However, when the in situ stress of 40 MPa is applied, the lining is completely broken. Assuming that the vertical in situ stress is calculated as $h\rho g$, where h is the depth of the tunnel, the depth corresponding to 56 MPa is approximately 2500 m. It can be concluded that the concrete lining might be unsuitable for deep underground engineering. To further investigate whether a higher grade of concrete will result in a better result, a computational model is simulated with a concrete lining of C100 concrete. Fig. 17 shows the numerical results. Although the three-point bending resistance of the high-grade concrete is higher, its in situ stress for lining cracking is not significantly different from that of the C60 concrete. As shown in Fig. 17, the cracking morphology of the C100 concrete lining under high in situ stress is significantly reduced (compared with that of the C60 concrete lining). Therefore, high-grade concrete is not good at preventing initial cracking but is good when the ultimate safety resistance is the main concern. From the numerical results, it is concluded that the in situ stress has a decisive influence on the cracking pattern of the concrete lining. In practice, the condition of the in situ stress could also be estimated based on the cracking morphology of the concrete lining. This example demonstrates that the quasi-brittle constitutive model can be used to study the cracking of concrete lining in underground engineering. Further research and development, into topics such as three-dimensional cracking, dynamic crack propagation and more detailed engineering scale verification, are necessary.

5. Conclusion

The DLSM is extended by the development of a new micro-mechanical constitutive model to predict quasi-brittle crack propagation in concrete. Even with considering the geometric non-uniformity and material heterogeneity, the original DLSM cannot reproduce the nonlinearity of the pre-peak hardening portion of the CMOD versus loading force curve and the dome morphology of the strain versus loading force curve observed in physical experiments. This can be resolved by using the newly developed constitutive model, which has three parameters, two of which are non-dimensional. In addition, a mathematical relationship between the micro-mechanical parameters of the model and the corresponding macroscopic material parameters of the concrete is established. The new quasi-brittle crack propagation model and parameter selection method have been proven to be applicable and effective from a detailed comparison between numerical and experimental results from the literature. By comparing the three-point bending experimental results, it is found that the constitutive model can successfully reproduce the pre-peak nonlinear portion of the loading and dome morphology of the strain-load curve. On this basis, the cracking of concrete lining is studied by considering the interaction between the in situ stress and concrete lining of different grades. The concrete grade has little effect on the initial cracking of the lining but has a significant impact on the ultimate failure of the lining. In addition, the direction of the in situ stress has a significant effect on the crack morphology and location. Therefore, in practice, the in situ stress of the tunnel might be estimated based on the crack morphology and location in the concrete lining.

Acknowledgements

This research is financially supported by the National Key Research and Development Program of China (2016YFC0401900) and the National Natural Science Foundation of China (Grant No. 1177020290).

References

Black, T., Belytschko, T., 1999. Elastic crack growth in finite elements with minimal remeshing. Int. J. Numer. Meth. Eng. 45 (5), 601–620.
Calayir, Y., Karaton, M., 2005. A continuum damage concrete model for earthquake analysis of concrete gravity dam-reservoir systems. Soil Dyn. Earthq. Eng. 25 (11), 857–869.
Cundall, P.A., 1971. A computer model for simulating progressive, large-scale movements in block rock systems. Symp. Int. Soc. Rock Mech. 1 (ii-b), 11–18.
Daux, C., Moës, N., Dolbow, J., Sukumar, N., Belytschko, T., 2000. Arbitrary branched and intersecting cracks with the extended finite element method. Int. J Numer. Meth. Eng. 48 (12), 1741–1760.
de Borst, R., 2002. Fracture in quasi-brittle materials: a review of continuum damage-based approaches. Eng. Fract. Mech. 69 (2), 95–112.
Dong, W., Wu, Z., Zhou, X., Wang, C., 2016. A comparative study on two stress intensity factor-based criteria for prediction of mode-i crack propagation in concrete. Eng. Fract. Mech. 158, 39–58.
Edalat-Behbahani, A., Barros, J.A.O., Ventura-Gouveia, A., 2017. Three dimensional plastic-damage multidirectional fixed smeared crack approach for modelling concrete structures. Int. J. Solid Strut. 115–116, 104–125.
Ghrib, F., Tinawi, R., 1995. An application of damage mechanics for seismic analysis of concrete gravity dams. Earthq. Eng. Struct. Dyn. 24 (2), 157–173.
Guanglun, W., Pekau, O.A., Chuhan, Z., Shaomin, W., 2000. Seismic fracture analysis of concrete gravity dams based on nonlinear fracture mechanics. Eng. Fract. Mech. 65 (1), 67–87.
Haeri, H., Sarfarazi, V., Zhu, Z., Hedayat, A., Nezamabadi, M.F., Karbala, M., 2018. Simulation of crack initiation and propagation in three point bending test using PFC2D. Struct. Eng. Mech. 66 (4), 453–463.
Huang, J.J., 2018. An incrementation-adaptive multi-transmitting boundary for seismic fracture analysis of concrete gravity dams. Soil Dyn. Earthq. Eng. 110, 145–158.
Jenq, Y.S., Shah, S.P., 1991. Features of mechanics of quasi-brittle crack propagation in concrete. Int. J. Fract. 51 (2), 103–120.
Jiang, C., Zhao, G.F., Khalili, N., 2017. On crack propagation in brittle material using the distinct lattice spring model. Int. J. Solids Struct. 118–119, 41–57.
Jiang, C., Zhao, G.F., 2018. Implementation of a coupled plastic damage distinct lattice spring model for dynamic crack propagation in geomaterials. Int. J. Numer. Anal. Meth. Geomech. 42 (4), 674–693.
Kazerani, T., Zhao, G.F., Zhao, J., 2010. Dynamic fracturing simulation of brittle material using the distinct lattice spring method with a full rate-dependent cohesive law. Rock Mech. Rock Eng. 43 (6), 717–726.
Kazerani, T., Zhao, J., 2010. Micromechanical parameters in bonded particle method for modelling of brittle material failure. Int. J. Numer. Anal. Meth. Geomech. 34 (18), 1877–1895.
Lee, J., Fenves, G.L., 1998. A plastic-damage concrete model for earthquake analysis of dams. Earthq. Eng. Struct. Dyn. 27 (9), 937–956.
Léger, P., Leclerc, M., 1996. Evaluation of earthquake ground motions to predict cracking response of gravity dams. Eng. Struct. 18 (3), 227–239.
Li, Q., Zhao, G.F., Lian, J., 2019. A fundamental investigation of the tensile failure of rock by using the three-dimensional lattice spring model. Rock Mech. Rock Eng. https://doi.org/10.1007/s00603-018-1702-z.
Mirzabozorg, H., Ghaemian, M., 2005. Non-linear behavior of mass concrete in three-dimensional problems using a smeared crack approach. Earthq. Eng. Struct. Dyn. 34 (3), 247–269.
Mridha, S., Maity, D., 2014. Experimental investigation on nonlinear dynamic response of concrete gravity dam-reservoir system. Eng. Struct. 80, 289–297.
Omidi, O., Lotfi, V., 2013. Continuum large cracking in a rate-dependent plastic-damage model for cyclic-loaded concrete structures. Int. J. Numer. Anal. Meth. Geomech. 37 (10), 1363.
Omidi, O., Valliappan, S., Lotfi, V., 2013. Seismic cracking of concrete gravity dams by plastic-damage model using different damping mechanisms. Finite Elem. Anal. Des.

63, 80–97.
Ooi, E.T., Natarajan, S., Song, C., Ooi, E.H., 2017. Crack propagation modelling in concrete using the scaled boundary finite element method with hybrid polygon–quadtree meshes. Int. J. Fract. 203 (1), 135–157.
Pan, J., Zhang, C., Xu, Y., Jin, F., 2011. A comparative study of the different procedures for seismic cracking analysis of concrete dams. Soil Dyn. Earthq. Eng. 31 (11), 1594–1606.
Potyondy, D.O., Cundall, P.A., 2004. A bonded-particle model for rock. Int. J. Rock Mech. Min. Sci. 41 (8), 1329–1364.
Rots, J.G., 1991. Smeared and discrete representations of localized fracture. Int. J. Fract. 51 (1), 45–59.
Stolarska, M., Chopp, D.L., Mos, N., Belytschko, T., 2001. Modelling crack growth by level sets in the extended finite element method. Int. J. Numer. Meth. Eng. 51 (8), 943–960.
Tang, C.A., Tang, S.B., Gong, B., et al., 2015. Discontinuous deformation and displacement analysis: From continuous to discontinuous. Sci. China Tech. Sci. 58 (9), 1567–1574.
Xu, T., Xu, Q., Tang, C.A., Ranjith, P.G., 2013. The evolution of rock failure with discontinuities due to shear creep. Acta Geotech. 8 (6), 567–581.
Wang, G.Y., Wang, W., Lu, M., Wang, C., 2017a. Deterministic 3D seismic damage analysis of Guandi concrete gravity dam: a case study. Eng. Struct. 148, 263–276.
Wang, S.Y., Sloan, S.W., Abbo, A.J., Masia, M.J., Tang, C.A., 2012. Numerical simulation of the failure process of unreinforced masonry walls due to concentrated static and dynamic loading. Int. J. Solids Struct. 49 (2), 377–394.
Wang, Y., Zhao, G.F., Yang, R., 2017b. Influence of empty hole on crack running in PMMA plate under dynamic loading. Poly. Test. 58, 70–85.
Wittmann, F.H., Rokugo, K., Brühwiler, E., Mihashi, H., Simonin, P., 1988. Fracture energy and strain softening of concrete as determined by means of compact tension specimens. Mat. Struct. 21 (1), 21–32.
Wu, Z., Xu, X., Liu, Q., Yang, Y., 2018a. A zero-thickness cohesive element-based numerical manifold method for rock mechanical behavior with micro-Voronoi grains. Eng. Anal. Boud. Elect. 96, 94–108.
Wu, Z., Ma, L., Fan, L., 2018b. Investigation of the characteristics of rock fracture process zone using coupled FEM/DEM method. Eng. Fract. Mech. 200, 355–374.
Zhao, G.F., 2017. Developing a four-dimensional lattice spring model for mechanical responses of solids. Comput. Meth. Appl. Mech. Eng. 315, 881–895.
Zhao, G.F., Fang, J.N., Zhao, J., 2012. A MLS-based lattice spring model for simulating elasticity of materials. Int. J. Comput. Meth. 09 1250037_01-22.
Zhao, G.F., Fang, J., Sun, L., Zhao, J., 2013. Parallelization of the distinct lattice spring model. Int. J. Numer. Anal. Meth. Geomech. 37 (1), 51–74.
Zhao, G.F., Fang, J., Zhao, J., 2011. A 3D distinct lattice spring model for elasticity and dynamic failure. Int. J. Numer. Anal. Meth. Geomech. 35, 859–885.
Zhao, G.F., Khalili, N., 2012. Graphics processing unit based parallelization of the distinct lattice spring model. Comput. Geotech. 42, 109–117.
Zhao, G.F., Xia, K., 2018. A study of mode-I self-similar dynamic crack propagation using a lattice spring model. Comput. Geotech. 96, 215–225.
Zhao, G.F., Yin, Q., Russell, A.R., Li, Y., Wu, W., Li, Q., 2019. On the linear elastic responses of the 2D bonded discrete element model. Int. J. Numer. Anal. Meth. Geomech. 43 (1), 166–182.
Zhu, W., Tang, C.A., Zhao, W., Teng, J., 2002. Numerical simulation on the fracture process of concrete specimen under static loading. Eng. Mech. 19 (6), 148–153.
Zhu, W., Tang, C.A., Liang, Z., Yang, T., 2004. Application of numerical test method to promote the teaching of rock mechanics experiment. Mech. Pract. 26 (2), 76–77.